Study of Wall Effects on an Eccentrically Moving Particle in a Cylindrical Channel

by

Rajib Kumar Saha

Submitted in partial fulfillment of the requirements for the degree of

MASTER OF SCIENCE IN MECHANICAL ENGINEERING

Department of Mechanical Engineering

BANGLADESH UNIVERSITY OF ENGINEERING AND TECHNOLOGY

Dhaka 1000, Bangladesh.

March, 2011

This thesis titled "**Study of Wall Effects on an Eccentrically Moving Particle in a Cylindrical Channel",** submitted by **Rajib Kumar Saha**, Student No. **0409102080F** Session April 2009 has been accepted as satisfactory in partial fulfillment of the requirement for the degree of MASTER OF SCIENCE IN MECHANICAL ENGINEERING on March 22nd , 2011.

BOARD OF EXAMINERS

1._____ Chairman

Dr. Noor Al Quddus
Assistant Professor,
Department of Mechanical Engineering
Bangladesh University of Engineering and Technology
Dhaka-1000, Bangladesh.

2._____ Member

Dr. Muhammad Mahbubul Alam (Ex-Officio)
Professor and Head,
Department of Mechanical Engineering
Bangladesh University of Engineering and Technology
Dhaka-1000, Bangladesh.

3._____ Member

Dr. M. Mahbubur Razzaque
Associate Professor,
Department of Mechanical Engineering
Bangladesh University of Engineering and Technology
Dhaka-1000, Bangladesh.

4._____ Member

Dr. Md. Mamun
Associate Professor,
Department of Mechanical Engineering
Bangladesh University of Engineering and Technology
Dhaka-1000, Bangladesh.

5._____ Member

Dr. A. K. M. Sadrul Islam (External)
Professor and Head,
Department of Civil and Environmental Engineering
Islamic University of Technology
Board Bazar, Gazipur-1704, Bangladesh.

CANDIDATE'S DECLARATION

It is hereby declared that this thesis or any part of it has not been submitted elsewhere for the award of any degree or diploma.

Signature of the Candidate

_____

Rajib Kumar Saha.

CERTIFICATE OF RESEARCH

This is to certify that the work presented in this thesis is carried out by the author under the supervision of Dr. Noor Al Quddus, Assistant Professor of the Department of Mechanical Engineering, Bangladesh University of Engineering and Technology, Dhaka, Bangladesh.

_____ _____

Dr. Noor Al Quddus Rajib Kumar Saha.

Dedicated to My Parents

ACKNOWLEDGEMENTS

I would like to thank my parents and my elder brother for giving me unquestionable support to continue my graduate study. I also want to express my gratitude to my uncle for giving me always supportive suggestions and inspirations in the course of my graduate study.

I want to express my gratefulness to my supervisor Dr. Noor Al Quddus who has guided me through the course of my graduate study and research. Without his guidance, support and suggestion this thesis was nearly unthinkable to complete. He has drawn my attention to various aspects of fluid mechanics and motivated me for the fundamental research work. I have benefitted enormously from our many discussions and his huge engagement in his students.

I want to extend my personal gratification to Prof. Sheikh Reaz Ahmed who has always given me the most useful advices for pursuing the M.Sc. degree. His sophisticated lectures on finite element method have benefitted me greatly. I give thanks to the lecturers Mahbubul Islam and Faruk Ahmed Sohag for their help in collecting different books from library.

ABSTRACT

This thesis deals with the effect of bounding wall on the Stokes drag for a spherical particle moving eccentrically inside a cylindrical channel. Numerous investigations were conducted in the past to find the increased drag for a particle flowing along the channel centerline. However, in reality particles may take any radial position inside the channel. This necessitates averaging the local enhanced drag coefficients for particles of all radial positions to get the resulting overall convective flux of the particle containing fluid. In this thesis, the values of local enhanced drag coefficients for an eccentrically moving spherical particle of different sizes and eccentric positions are quantified.

A general three dimensional finite element particle transport model consisting of Navier-Stokes and continuity equations defined in arbitrary Lagrangian-Eulerian kinematics has been developed to study the motion of a rigid uncharged spherical particle moving eccentrically inside a cylindrical channel. Wall correction factors and lag factor have been calculated in the Stokes flow regime ($Re < 1$) covering the range of particle to channel radii ratio, $0.2 \leq \lambda \leq 0.9$ and eccentricity, $0 \leq e \leq 0.8$, where, $\lambda = a/r_0$, $e = d/(r_0 - a)$ and a, r_0, and d represent particle radii, channel radii, and displacement of particle center from the channel centerline, respectively. Three different flow situations have been considered: i) steady particle motion in an otherwise quiescent fluid, ii) particle held fixed in a Poiseuille flow, and iii) freely suspended particle in a pressure driven flow.

The unique feature of this model is that, it directly provides precise quantitative insight about how slow a particle moves compared to the surrounding fluid i.e. the lag factor at any eccentric position inside the channel. The calculated values match closely with the results obtained by lubrication theory for higher eccentric positions. However, with the increase of surface to surface separation distance at lower eccentric positions and lower particle to channel radii ratio the present model shows deviation from results obtained by lubrication theory.

TABLE OF CONTENTS

NOMENCLATURE

Notation	Definition
ρ	Density of the fluid
μ	Dynamic viscosity of the fluid
υ	Kinematic viscosity of the fluid
V_{max}	Maximum centerline velocity of fluid in a Poiseuille flow
V_m	Mean velocity of the fluid in channel
a	Radius of the spherical particle
r_0	Radius of the cylindrical channel
r_{res}	Radius of the reservoir
d	Distance of the particle center from the channel axis
h	Separation distance of the particle from the channel wall
e	Eccentricity of the particle inside the channel
λ	The ratio of the particle and channel radius
K_1, K_2	Wall correction factors
G	Lag factor
$\boldsymbol{u}$	Velocity vector of the fluid
u, v, w	Velocity components in x, y and z direction respectively
U_p	Velocity of the particle
p	Pressure of the flowing fluid at any point within the channel
$\boldsymbol{F_b}$	Fluid body force
τ_{ij}	Viscous stress tensor
σ_{ij}	Total stress tensor
Re	Reynolds number
Φ, φ, ψ	Mapping functions for transforming different co-ordinate systems in ALE description
$x, X, \boldsymbol{\chi}$	Symbols used in ALE description to denote co-ordinate points at spatial, material and referential domains respectively
$R_{\boldsymbol{x}}, R_{\boldsymbol{X}}, R_{\boldsymbol{\chi}}$	Symbols for different reference domains in ALE description
Ω	Fixed frame of reference
$\overline{\Omega}$	Moving Mesh frame
ψ_m	Mesh velocity
ψ_{mx} , ψ_{my} , ψ_{mz}	Mesh velocity in x, y and z directions respectively
$\hat{u}$	Shape function for x component of velocity
$\hat{p}$	Shape function for pressure
$\hat{\mathrm{x}}_{\mathrm{i}}$	Shape function for coordinates in moving mesh frame

LIST OF TABLES

Table No. **Page No.**

LIST OF FIGURES

Figure No. **Page No.**

1. INTRODUCTION

1.1 Background and Motivation

Numerous engineering applications involve fluid flow containing suspended particles and require particle filtration. The diversity of such applications may be illustrated by a few examples: membrane filtration, the characterization of hemodialysis membranes, the modeling of size-exclusion and hydrodynamic chromatography, the determination of an optimal pore size for supported catalysts, DNA and protein separations, porous media flow and blood flow modeling [1-3]. To understand the separation technique of these filtration membranes, the hindered transport theory has been extensively investigated. It is well known that solutes in liquid filled pores of molecular dimensions have reduced diffusivities. For large solute molecules that are in the order of channel radius in size, this hindered transport can be explained by a combination of the particle-wall hydrodynamic interactions and steric restrictions. This phenomenon has been studied both theoretically and experimentally in past, to understand the effect of size of the solute particles on membrane permeability.

The description of membrane transport in terms of a series of parallel pores of cylindrical shapes has received considerable attention over the years. Modeling the pores as the summation of parallel cylinders has significant benefit as it requires only analyzing the problem of a single particle in a single cylindrical channel. The fundamental research on the hydrodynamic interaction of spherical particle moving through liquid filled channel is comprehensively investigated in the past.

The effect of the vicinity of the wall on the particle motion is usually characterized in terms of dimensionless wall correction factors and lag factor. Wall correction factor is the ratio of the drag force encountered by a moving particle through a liquid filled channel to the drag force experienced when moving through unbounded liquid. Lag factor is the ratio of the steady velocity of particle to the velocity of the fluid in absence of particle. This defines how slow a particle moves relative to the flowing fluid. The vicinity of the particle surface to the channel wall is characterized by the particle to channel radii ratio $\lambda\ (= a/r_0)$, where, a = particle radii, r_0 = channel radii and the eccentricity e of the particle is defined as, $e = d/(r_0 - a)$, here, d = displacement of particle center from the channel centerline.

The wall correction factors and lag factor for a rigid spherical particle flowing along the channel centerline is available in the literature for a variety of flow situations. Both analytical and numerical calculations were reported for the centerline motion of the particle through the channel, and those results were later verified by experimental results. However, in real applications e.g. protein transports, DNA separation, blood flow simulation, particles may take any radial position inside the channel. This necessitates averaging the local enhanced drag coefficients for particles of all radial positions to predict the resulting overall convective flux of the particle containing fluid.

So, the values of local enhanced drag coefficients for an eccentrically positioned spherical particle of different sizes should be precisely quantified. Literature provides some attempt to model the flow of eccentrically moving particle inside the channel. However, the analysis was limited to very small particles where the particle separation from the channel wall is higher compared to its radius [4]. Another attempt was made to find the dependence of the particle drag on its lateral position [5]. However, no exact quantification was presented. A numerical approach, namely the spectral boundary element method was used to find the wall correction factors and lag factor for an eccentrically flowing particle inside the channel [6].

These investigations have been done using the linear Stokes equation with the complete omission of the nonlinear inertia term in the Navier-Stokes equation. At very low Reynolds number, this is a rational choice as the inertia effect is negligible compared to the viscous effect at this flow region. However, this limits the analysis to be performed at very low Reynolds number only. In this thesis, the full Navier-Stokes equation is solved, considering the inertia effects on the particle motion. This facilitates analyzing the wall effects on the particle motion at any Reynolds number, utilizing the same model. Advantage is taken of the linearity of the Navier-Stokes equation at low Reynolds number to get the full description of the problem from linear superposition of two different simpler ones.

In conventional fluid mechanics problems governing Navier-Stokes equation is usually solved in Eulerian framework. In this description the frame of reference remains fixed in space and the continuum moves with respect to the reference frame. However, presence of the moving particle within the fluid results in a geometrical domain which deforms with time. This prevents defining the Navier-Stokes equation in purely Eulerian framework. On the other hand, the large distortion of the material resulting from the fluid motion makes the Lagrangian description unsuitable. So, a new kinematical description is utilized in the present research which is known as arbitrary Lagrangian Eulerian (ALE) description [7]. In ALE description, the frame of references i.e. the mesh nodes on the computational domain can be held fixed in a pure Eulerian way or can be allowed to move with the deforming continuum in Lagrangian fashion at certain interfaces, or can be given some arbitrary velocity with respect to the deforming material. The motion of the moving particle is tracked by the Lagrangian framework and the position of the computational grid and the associated flow field variables are updated after each time step. Simulating the movement of the particle through liquid filled channel is not possible by the Lagrangian or Eulerian methods independently. This method has overcome this limitation.

The off-centerline position of the particle prevents axi-symmetric analysis of the problem. A three dimensional geometric model is utilized to obtain the solution for eccentric motion of a particle in the cylindrical channel. A commercial finite element package is used. Total drag force on the particle is calculated by integrating the stress tensor on the particle surface. The calculated drag force is used to find the wall correction factors and lag factor of the particles.

1.2 Objective of the Thesis

The specific objectives of this thesis are as follows:

(a) To develop a 3-D finite element model consisting of Navier-Stokes and continuity equations defined in arbitrary Lagrangian-Eulerian (ALE) kinematics to study the motion of rigid, uncharged spherical particles moving through liquid filled cylindrical microchannel.

(b) To study the wall effect on the eccentrically moving particle in a cylindrical microchannel. Three flow situations are considered:

Case-I: considers the translation of the spherical particle parallel to the channel axis with a uniform velocity in an otherwise quiescent fluid. The wall correction factor determined in this case is termed as K_1.

Case-II: considers a fixed spherical particle in a Poiseuille flow at different radial positions of the cylinder. Wall correction factor determined in this case is termed as K_2.

Case-III: considers a spherical particle suspended in the Poiseuille flow and free to move with the fluid. From this analysis the lag factor G can be directly determined.

(c) To calculate the wall correction factors and lag factor of a spherical particle moving eccentrically in a cylindrical channel for different particle to channel radii ratios ($0.2 \leq \lambda \leq 0.9$) and different eccentric positions ($0 \leq e \leq 0.8$).

1.3 Outline of the Thesis

A detail literature review is provided in Chapter 2. The theoretical description of the model is described in Chapter 3. The particle-channel geometrical configuration, the governing equations for fluid flow, arbitrary Lagrangian Eulerian kinematics of particle movement, boundary conditions, non-dimensionalization of the model, and calculation procedure of wall correction factors are described. In Chapter 4, numerical solution methodology of the model is described. A brief description of the procedure involved in finite element analysis along with the weak form formulation of Navier-Stokes equation, continuity equation and mesh smoothing equation is provided. Procedure for implementing the solution methodology i.e. meshing, shape functions, algebraic equation solving techniques etc. are delineated. A flowchart of the overall solution methodology is also provided. Chapter 5 presents the simulation results. First the model is validated by comparing the calculated wall correction factors of a spherical particle flowing along the channel axis, against existing analytical and numerical results found in the literature. In the later sections, the values of the wall correction factors are presented for spheres of different sizes, moving at different radial positions inside the channel. In Chapter 6, the conclusion and the recommendations for future works are presented.

2. LITERATURE REVIEW

Transport of particles through microscopic pores filled with viscous fluid plays an important role in many engineering disciplines. The maximum achievable flux for particle-containing fluid through microscopic channel is found significantly less than the pure fluid flux. The rate of convective transport of the solute particles is found to be lower than the product of bulk solute concentration and fluid flow rate. In absence of channel fouling, this hindered transport results entirely from the hydrodynamic retardation effect on the moving particle due to the proximity of wall. Extensive studies on this topic by different researchers are reviewed in literature [8-9].

Different theoretical methods have been introduced to explain this hindered transport phenomena. Most investigators have modeled the pores as the summation of parallel cylinders. As a result, in most of the cases, the motion of a single particle in a cylindrical channel is analyzed. Another simplification is done by assuming the particle motion to be along the axis of the cylinder that reduces the problem from three dimensional analysis to two dimensional axi-symmetric analysis. The effect of proximity of the cylinder walls on the drag of an axially moving sphere was initially analyzed using the method of reflection [10]. In this method, starting with the known solution for the drag of a rigid sphere in an unbounded medium i.e. the Stokes solution, a 'reflection flow' is superposed such that the boundary conditions on the sphere are satisfied exactly. The drag of the sphere is obtained from Stokes law using the velocity of the sphere increased by the average 'reflection' velocity on the sphere. Approximate expression for the drag of the rigid spheres was given.

An exact solution for the wall correction factors for the axial motion of rigid spheres in stationary and moving liquids within an infinitely long cylindrical channel has been obtained in terms of an infinite set of linear algebraic equations for the coefficients of Stokes stream functions [11]. In this analysis, it was pointed out that, the drag of a sphere in motion within a moving liquid is composed of two parts: namely, the drag due to the motion of the sphere in a quiescent liquid inside the cylindrical tube, and the drag due to the motion of the liquid within the cylindrical tube. Both cases were analyzed for rigid spheres and fluid spheres (i.e. spheres which have different physical properties than the external fluid and are characterized by internal motion). However, the provided solution for the fluid spheres was approximate. Moreover, the results of the wall correction factors of particles they provided were limited to the ratios of particle to channel radii $\lambda \leq 0.8$, where $\lambda = a/r_0$ and a and r_0 are the particle and channel radii, respectively.

The change in the different aspects of the behavior of the flowing suspended particles due to change in particle size and shape and flow induced deformation was investigated [4]. The analysis was done using the linear creeping flow equations for very small particles i.e. $\lambda << 1$. Method of reflection was used to find the additional pressure drop

required for a single spherical particle in a Poiseuille flow. Eccentrically moving particles was also considered for cases where the particle separation from the tube walls is large compared to the particle radius. It was pointed out both theoretically and experimentally that, due to the linearity of the creeping flow equations, radial migration of an eccentrically moving particle can be neglected, but at higher Reynolds number, due to the presence of nonlinear inertia force, particles have a tendency to move radially across streamlines. Experimental evidences were presented to state that, a neutrally buoyant sphere migrates towards a position of stable equilibrium at a distance of $0.5r_0$ to $0.6r_0$. Deformations of deformable fluid drop and flexible filaments, and effect of unsteady flow thorough cylindrical tube were also discussed.

Singular perturbation techniques was used to investigate the slow, asymmetric flow around a sphere positioned eccentrically within a viscous liquid filled long, circular, cylindrical channel [5]. They provided wall correction factors for the axially flowing spherical particle accurately for all λ values ($0 \leq \lambda \leq 1$). The obtained results covered the situations in which the sphere occupies virtually the entire cross section of the cylinder, so that the clearance between the particle and tube wall was everywhere small compared with both the sphere and tube radii which eventually presented an improved version of the conventional "lubrication-theory" analysis. Asymptotic expansions, valid for small dimensionless clearances were obtained for the hydrodynamic force, torque and pressure drop for flow past a stationary sphere, and for a sphere translating or rotating in stationary fluid. However, the dependence of drag force on the spherical particle upon its lateral position was represented by an undetermined function. Change in the translational velocity for a sphere in a Poiseuille flow with its eccentric position was predicted. It was stated that, displacement of the sphere to eccentric position decreases its velocity only slightly, unless eccentricity is very close to unity. The sphere translates faster than the mean fluid velocity for most eccentric positions. Lateral displacement of the sphere from the concentric position leads to a considerable increase in additional pressure drop, all other things being equal. Sedimentation of a sphere in a vertical tube was also analyzed. It was found that, the settling velocity increases monotonically with lateral position until the eccentricity equals to 0.98.

The governing hydrodynamic equations of transport through microchannel were re-examined and necessary conditions for a simplified, one-dimensional treatment of the diffusion and convection processes were established [12]. Both empirical and theoretical approaches were carried out and wall correction factors for the centerline motion of a rigid spherical particle were calculated for $0 \leq \lambda \leq 0.9$ [13]. These were the more accurate values of these factors than calculated by [11].

The objective of the above mentioned research works on hindered transport was to predict transport coefficients from the information of size, shape and electrical charge of the solute particles and pores. The theoretical development of diffusive and convective transport of dilute solutions of neutral spheres in cylindrical pores is reviewed and extension of this basic theory including electrostatic interactions, non-spherical solutes, pore shapes other than cylindrical and finite solute concentration is discussed [8].

First numerical investigation of this topic was initially performed using the finite element method to calculate the wall correction factors for single particle and short chain of particles flowing along the axis of the cylinder [14]. The values of the wall correction factors were obtained for $\lambda \leq 0.8$. Limiting particle spacing for short chain of particles was found, for which single sphere approximation gives accurate results for the inner spheres of the particle chain. It was shown that, single sphere calculations have a wide range of applicability, which simplifies the effort involved in numerical calculations considerably. The calculated values of the wall correction factors were used to evaluate the maximum achievable flux of a particle containing fluid through a micro-porous membrane. In extension of this analysis, the same researchers have included the electrostatic effect with the pure hydrodynamic retardation effect to find the forces on a charged spherical particle as a function of distance of approach and entry to a charged cylindrical channel in a charged planar surface [15]. Galerkin finite element scheme was implemented for getting the numerical solution of the nonlinear Poisson-Boltzmann and Navier-Stokes equations for electrostatic interaction and hydrodynamic interaction, respectively.

The resistance force for a torque free spherical particle flowing eccentrically inside a cylindrical channel was first analyzed numerically [6]. Stokes equation with the boundary conditions was formulated using the boundary integral method. The boundary integral equation was numerically solved by spectral boundary element method. They have considered rigid solid spheres, fluid droplets and bubbles. A lubrication theory was also presented for predicting the limiting resistance of bodies near contact with the cylindrical walls. The calculated numerical data was represented by algebraic expressions for entire eccentricity values ($0 < e < 1$) and for all particle sizes ($0 < \lambda < 0.9$). The numerical coefficients in these algebraic expressions were obtained from the detailed computational results together with known asymptotic limits.

Lattice-Boltzmann method was used to calculate the total hydrodynamic force and the wall correction factors for a sphere flowing inside an orthogonal circular cylinder and in a prismatic enclosure with various rectangular cross-sections [16]. Wall correction factors for the centerline motion of the sphere in the creeping flow region were obtained for $\lambda \leq 0.8$. The effect of inertia on the particle motion was also determined by computing the hydrodynamic force at several values of the Reynolds number. Off-center settling of a solid sphere was also investigated. Using direct numerical simulation, considering the inertia effect, they have found that there exists a lateral force on the eccentrically moving particle for finite Reynolds number flows. This lateral force combined with the viscosity of the fluid, results in damped oscillations around the channel axis and the particle finally settles along the centerline. They have also found that when the Reynolds number is very small but finite, particle simply approaches the centerline and then settles there. For higher Reynolds number, the lateral oscillation of the particle is more significant. Another observation was that, more confined space in cylindrically channel generates a stronger lateral force on the sphere.

Numerical and asymptotical investigations were performed on the influence of uniform and Poiseuille flow on the wall correction factor of spherical particle placed at the axis of the channel [17]. The Stokes and continuity equations were expressed in terms of the stream function and vorticity formulation and were solved using finite difference method. In all the numerical computations they have calculated the separate contributions of the pressure and viscosity forces. This calculation was in good agreement with those obtained by asymptotic expansions. They have pointed out the prevalence of the pressure term over the viscosity term in the lubrication regime (very high λ values) which is opposite to what happens for dilute regime. The calculated wall correction factors covered the entire range of particle sizes, i.e. $0 < \lambda < 1$.

Most recent status on the development of hindered transport theory was reviewed for neutral spheres in long pores of cylindrical and rectangular cross section [9]. Diffusive and convective hindrance factors for macroscopic fluid flux are derived for uncharged spherical particles. However, the theory presented was for dilute solutions. Expressions for diffusive and convective hindrance factors were provided by utilizing the cross sectional averaging of local enhanced drag coefficients. They have employed the previously found results of local enhanced drag coefficients available for centerline approximation and eccentric particle positions found from [6]. Comparisons were made between the updated theory and recent experimental data.

A finite element particle transport model consisting of Navier-Stokes and continuity equations defined in arbitrary Lagrangian Eulerian kinematics was employed to describe the axial motion of a rigid uncharged spherical particle in an infinitely long cylindrical channel of uniform cross-section [19]. Wall correction factors were calculated covering the entire particle size range ($0 < \lambda < 1$). Finite channel length effects on the motion of the particle were also investigated. These are particle transport at the channel entry and the exit from the reservoir and motion of a particle in a dead end under the influence of an external force. This model directly provides the lag factor G which is a unique feature of it, as the lag factor was previously determined separately by calculating the wall correction factors. Therefore, this model provides a self consistent solution of the particle transport in the cylindrical capillary including the complete hydrodynamic interactions between the particle and channel wall.

Evidences of experimental investigations to find the hydrodynamic interactions between the particle and the bounding wall and also between individual particles are found in literature [20-22]. The major difficulty in the experimental determination of the hydrodynamic interactions between individual particles and of the presence of bounding walls arises due to the fact that, controlling the spatial position of the particle becomes difficult as the particle either move due to the presence of external force field or imposed velocity field. However, different experimental techniques have been developed. Sphere rheometer was used to study the effect of wall on the hydrodynamic force exerted on a sphere moving parallel to it at a constant velocity. Particle-tracking experiments were performed to study the motion of a particle in a low-Reynolds-number Poiseuille flow between two parallel plane walls considering neutrally buoyant

spherical particles for particles sizes up to $\lambda = 0.95$ [22]. Translational velocities of particles and their distribution across the channel was found out. Non spherical particles such as, cubes, parallelepipeds, cylinders, needles, thin plates and circular discs of different sizes was also considered [23]. The wall correction factors and lag factors were calculated for the low Reynolds number flow ($Re < 7$). These experimental results confirm the theoretically and numerically computed values.

Although the study of wall correction factors has reached a very mature state, the effect of wall on an eccentrically moving particle at any finite Reynolds number, have not been exactly quantified. The only available data for the wall correction factor for this case was determined by solving the linear Stokes equation [6]. They have employed the boundary integral method for Stokes equation to calculate the values of wall correction factors, which neglects the inertia effect on the particle motion in the close proximity of the wall. However, for finite values of Reynolds number the inertia effect cannot be totally neglected. This warrants a general numerical scheme which includes the inertia effect, thus allowing calculation of wall correction factor at any Reynolds number in the laminar flow regime. In this thesis, a general numerical model is presented which considers the full Navier-Stokes equation to include the inertia effect for calculating wall correction factor of an eccentrically moving spherical particle inside a cylindrically channel. This model can be employed to find out the wall correction factor and lag factor for particles of any shape, size and position at any Reynolds number within the laminar flow region.

3. THEORETICAL DESCRIPTION OF THE MODEL

3.1 Model Geometry

An infinite channel is modeled as a cylindrical channel of finite length L_{ch} and of uniform radius r_0 having reservoirs at both ends, as shown in Fig. 3.1. The reservoir radius r_{res} is taken to be five times larger than the channel radius. The channel length is taken sufficiently long (20~50 times r_0) so that the effect of the channel ends on the particle motion can be neglected at the center of the channel. The fluid having density ρ and dynamic viscosity μ flows inside the channel due to the applied pressure gradient. In this analysis, a uniform velocity profile is applied at the reservoir inlet and the outlet of the fluid receiving reservoir is set as a zero total stress condition, which implies un-restrained channel end.

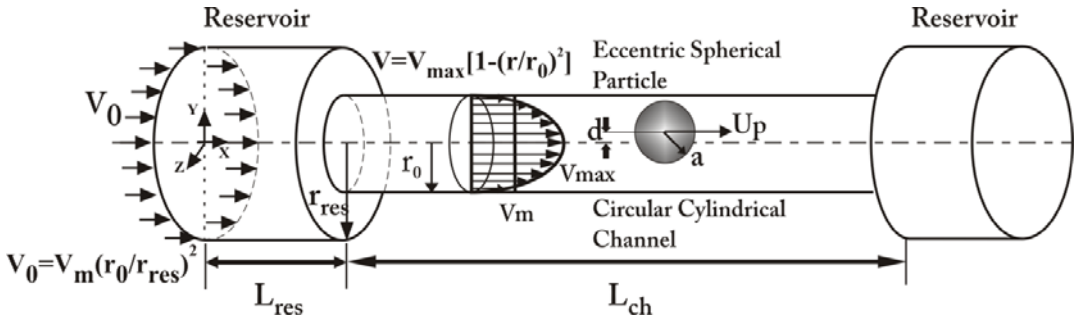

Fig. 3.1: Schematic depiction of the model geometry

The laminar boundary layer from the channel wall will merge at a distance of $\acute{L}$ from the channel entrance and a fully developed flow i.e. Poiseuille flow will be generated, where $\acute{L}$ [24] is given by,

$$\acute{L} = 0.058 * Re_D * D \tag{3.1}$$

and, Re_D is the Reynolds number based on channel diameter, and D is the channel diameter. For the Poiseuille flow the velocity profile takes a parabolic shape which can be represented by the following equation,

$$v = -\frac{1}{4\mu}\frac{dp}{dx}({r_0}^2 - r^2) \tag{3.2}$$

where, $\frac{dp}{dx}$ is the applied pressure gradient and v is the fluid velocity at radial distance r from the channel axis. At the center of the channel (at $r = 0$) maximum velocity is achieved which is denoted as V_{max}. The mean velocity V_m for a parabolic velocity profile is equal to half of this maximum velocity, i.e. $V_m = V_{max}/2$. The velocity profile in the fully developed flow region found from the numerical computation is compared with the velocity profile from the above equation to validate the accuracy of this finite channel length approximation. A spherical particle having radius a is placed

at the mid-way along the length of the cylinder. Thus it is ensured that the particle is in the fully developed flow region and also effects from the channel entrance and exit on the particle motion will be minimum.

The presence of the particle will disturb the Poiseuille flow and an additional pressure will be required to sustain the flow. The main driving force for the particle is the applied pressure and the hydrodynamic drag force acts on it as a resistance to its flow. For a non-accelerating particle, these two forces will reach an equilibrium and the particle will attain a uniform velocity U_p. However, the particle velocity will not be equal to the fluid velocity; specifically it will be somewhat lower than the undisturbed fluid velocity which will be discussed later in detail.

During the flow inside the channel, the particle takes different radial position i.e. eccentric positions from the channel axis. The eccentricity of the particle is denoted by e and is expressed as:

$$e = \frac{d}{r_0 - a} \tag{3.3}$$

where d is the distance of the particle center from the channel axis. The minimum and maximum value of d can be zero and $(r_0 - a)$, respectively. So, the range of this eccentricity value becomes $0 < e < 1$. The analysis is done for different $\lambda\ (= a/r_0)$ values ($0.2 \leq \lambda \leq 0.9$) and eccentricity values ($0 \leq e \leq 0.9$).

3.2 Governing Equations for Fluid flow

The momentum conservation of an incompressible Newtonian fluid in the continuum approximation in Eulerian framework is described by the Navier-Stokes equation,

$$\rho \frac{\partial \boldsymbol{u}}{\partial t} + \rho \boldsymbol{u} \cdot \nabla \boldsymbol{u} = -\nabla p + \mu \nabla \cdot (\nabla \boldsymbol{u} + \nabla \boldsymbol{u}^T) + \boldsymbol{F}_b \tag{3.4}$$

where the first term in the left side of the equality sign is the unsteady term and the second term is the nonlinear inertia term. The first term at the right of the equality sign denotes pressure gradient, the second term denotes the viscous force i.e. dynamic viscosity $\boldsymbol{\mu}$ multiplied by gradient of viscous stress tensor $\boldsymbol{\tau_{ij}}$, and the third stands for body force such as gravity, electrical forces. In this analysis, the body force of the fluid is not considered. However this term will not be discarded during the theoretical description of the model. With total stress tensor notation the Navier-Stokes equation becomes,

$$\rho \frac{\partial \boldsymbol{u}}{\partial t} + \rho \boldsymbol{u} \cdot \nabla \boldsymbol{u} = -\nabla \cdot \boldsymbol{\sigma_{ij}} + \boldsymbol{F}_b \tag{3.5}$$

where the total stress tensor $\boldsymbol{\sigma_{ij}}$ equals,

$$\boldsymbol{\sigma_{ij}} = -p\bar{\bar{\mathrm{I}}} + \mu(\nabla \boldsymbol{u} + \nabla \boldsymbol{u}^T) \tag{3.6}$$

and $\bar{\bar{I}}$ is the identity tensor. As in this analysis three dimensional analysis is performed, here the elaborated form of the total stress tensor for three space dimensions is illustrated:

$$\boldsymbol{\sigma_{ij}} = \begin{bmatrix} 2\mu\frac{\delta u}{\delta x} - p & \mu\left(\frac{\delta u}{\delta y} + \frac{\delta v}{\delta x}\right) & \mu\left(\frac{\delta u}{\delta z} + \frac{\delta w}{\delta x}\right) \\ \mu\left(\frac{\delta v}{\delta x} + \frac{\delta u}{\delta y}\right) & 2\mu\frac{\delta v}{\delta y} - p & \mu\left(\frac{\delta v}{\delta z} + \frac{\delta w}{\delta y}\right) \\ \mu\left(\frac{\delta w}{\delta x} + \frac{\delta u}{\delta z}\right) & \mu\left(\frac{\delta w}{\delta y} + \frac{\delta v}{\delta z}\right) & 2\mu\frac{\delta w}{\delta z} - p \end{bmatrix}$$

where $u, v,$ and w denote the fluid velocity components in x, y and z coordinate directions, respectively. This expression for the total stress tensor is used to determine the total force on the particle due to its relative motion to the fluid.

To ensure the conservation of mass, continuity equation needs to be considered,

$$\frac{\delta\rho}{\delta t} + \nabla \cdot (\rho \boldsymbol{u}) = 0 \tag{3.7}$$

As the fluid is considered incompressible, the time derivative of the density term vanishes and the continuity equation becomes,

$$\nabla \cdot \boldsymbol{u} = 0 \tag{3.8}$$

A very common way of simplifying the Navier-Stokes equation at very low Reynolds number region ($Re << 1$) is complete omission of the inertia force of the fluid arising from its velocity. At very low Reynolds number, the fluid velocity is very small, so the resulting inertia forces are comparably small in terms of viscous forces. This simplification results in creeping flow or Stokes equation. Since the only non-linear term in the Navier-Stokes equation is the inertia term there is substantial benefit of this simplification because the resulting equation is linear. That means, if (v_1, p_1) and (v_2, p_2) separately satisfies this linear equations then (v_1+v_2, p_1+p_2) will also satisfy the equation. So by applying the classical superposition technique of linear partial differential equation, solution of a complex problem can be found by splitting the problem into simpler ones and superposing those solutions linearly.

In this analysis, the Navier-Stokes equation is used, although the inertia effects are negligible. However, to analyze the problem the linearity of the equation is taken as an advantage. The problem considered here involves analyzing motion of a spherical particle flowing eccentrically through a cylindrical channel. This problem is split up into simpler ones, which are: Case-I: fixed particle in a moving fluid, and Case-II: moving particle in a stationary fluid. A complete description of the problem can be found by analyzing these two cases separately.

However, this simplification is only valid when the Reynolds number is near to zero. In practical cases for higher Reynolds number, inertia effects cannot be neglected, which inhibits the linear superposition of the separate results. So, another case i.e. Case-III is developed, which considers a spherical particle suspended in the Poiseuille flow and free to move with the fluid. From this analysis the lag factor *G* is directly determined. The result from this third case is used to validate that; the results from the first two cases can be confidently employed to get the full description of the problem at very low Reynolds number. Moreover, this model can be employed for high Reynolds number flows in the laminar region.

3.3 Calculation of Wall Correction Factors

G. G. Stokes first derived the drag on a spherical particle moving with a uniform velocity U_p in an unbounded stationary fluid by solving the creeping flow equations, given by:

$$F_\infty = 6\pi\mu a U_p \tag{3.9}$$

For the particle motion in a region bounded by channel wall the value of this drag force increases. This increased drag is usually characterized by two wall correction factors. The first situation (Case-I) considers a uniformly moving particle through a stationary fluid. In this case the ratio of the actual drag to the Stokes drag is termed as wall correction factor K_1. If the value of the actual drag force in this case is F_1, K_1 can be expressed as:

$$k_1 = \frac{F_1}{F_\infty} \tag{3.10}$$

which yields:

$$F_1 = k_1 6\pi\mu a U_p \tag{3.11}$$

The second situation (Case-II) considers a stationary particle held fixed in a moving fluid. This wall correction factor is termed as K_2. In case of pressure driven flow the drag on the particle is calculated in terms of the maximum velocity V_{max} inside the channel. If the value of the actual drag force in this case is F_2, K_2 can be expressed as:

$$k_2 = \frac{F_2}{F_\infty} \tag{3.12}$$

which yields:

$$F_2 = -k_2 6\pi\mu a V_{max} \tag{3.13}$$

The minus sign accounts for the fact that, in this case the direction of the force exerted by the flowing fluid on the particle is opposite to that found from the previous case. As previously mentioned, due to the linearity of the Navier-Stokes equation in the Stokes flow regime the particle-wall hydrodynamic interaction in a pressure driven flow can be

expressed as linear superposition of this two cases. So, the drag on a moving particle in a flowing fluid is expressed as:

$$F_3 = 6\pi\mu a(k_1 U_p - k_2 V_{max}) \tag{3.14}$$

The net force acting on a uniformly moving particle inside a flowing fluid should be zero because of its zero acceleration. By setting the value of the force F_3 to be zero Equation 3.14 yields:

$$U_p = \frac{K_2}{K_1} V_{max} = G\, V_{max} \tag{3.15}$$

here the new parameter G is called lag factor. The physical significance of this factor suggests how slow a particle moves with respect to the flowing fluid. Most studies in literature presents the hydrodynamic interactions in terms of either K_1 and K_2 or K_1 and G. These three factors are dependent on the parameter λ and eccentricity e of the particle inside the channel.

In this thesis, the values of K_1 and K_2 are determined by considering two different cases (Case-I and Case-III) as mentioned above. However, from the third case which considers a moving particle in a moving fluid the value of the lag factor can be directly calculated by taking ratio of the particle velocity and the undisturbed fluid velocity along the axis of the channel, V_{max}.

3.4 Necessity of Arbitrary Lagrangian Eulerian (ALE) Method

To have a clear delineation of the fluid-solid surfaces where large distortion of the continuum under consideration is present, it is very important to have an appropriate kinematic description of the continuum. This kinematic description should give a relationship between the deforming continuum and the computation domain which can be used for solving the equations. In general classical Eulerian and Lagrangian description of the continuum are used though both of them have some advantages and limitations which are discussed in the following paragraphs.

Eulerian description is widely used in fluid mechanics and is very efficient when the computational domain remains fixed with time. In this description the frame of reference remains fixed in space and the continuum moves with respect to this. Large distortion of the continuum motion can be handled properly but as the frame of reference remains fixed with time it cannot handle the scenario where the geometrical domain under consideration is deforming with time. In this thesis, in Case-II, the analysis involves a stationary particle held fixed at some point in a Poiseuille flow. As the geometrical domain considered here is not changing with time, a pure Eulerian description of the governing equations can be used. However, Case-I involves analyzing a uniformly moving particle in a stationary fluid, where the geometrical domain is changing with time due to the change in particle position, Eulerian description of the governing equations cannot be used.

On the other hand, in pure Lagrangian description each individual material particle is tracked or followed to define the overall state of the moving continuum. This method is generally used in solid mechanics problems where material deformation is small. But in the problems considered here, a large distortion of the material is resulted due to the fluid motion, which makes this Lagrangian description unsuitable. The advantages of Lagrangian description is, it facilitates clear definition of interfaces of different materials e.g. particle surface.

Both of the Eulerian and Lagrangian description have some limitations and specific advantages. However, neither of those can be employed individually to handle a time dependent geometrical domain involved in this analysis. Another kinematical description which uses the best features of each of this method is the arbitrary Lagrangian Eulerian (ALE) description [7]. In this method, the frame of references i.e. the mesh nodes on the computational domain can be held fixed in a pure Eulerian way or can be allowed to move with the deforming continuum at certain interfaces in Lagrangian fashion or can be given some arbitrary velocity with respect to the deforming material. The comparison between these three descriptions can be understood from a one dimensional case shown in the figure below:

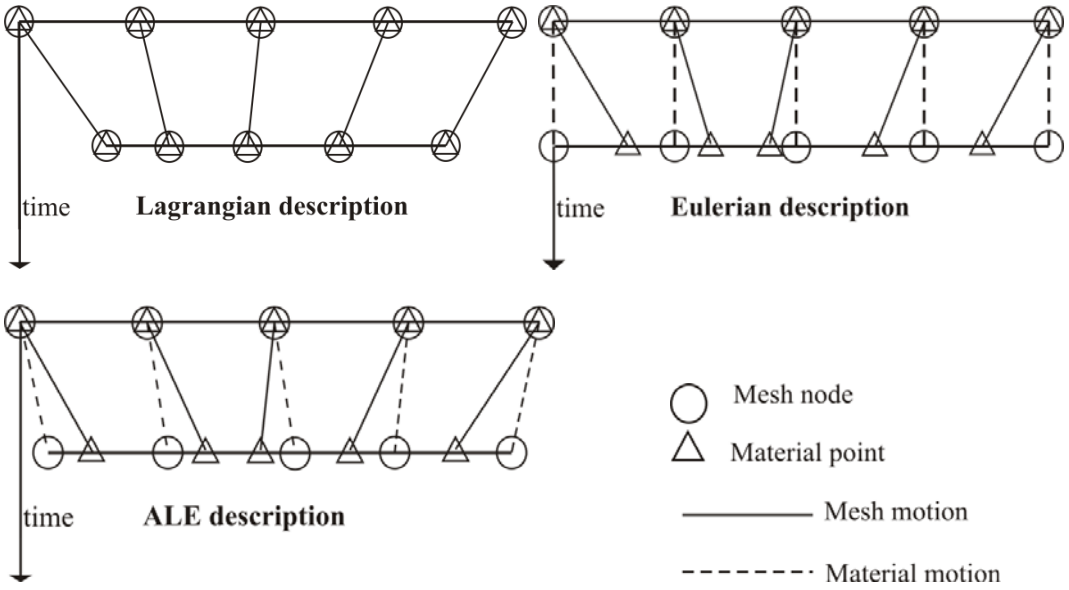

Fig. 3.2: Comparison of Lagrangian, Eulerian and ALE description

In Lagrangian description, as shown in Fig. 3.2, the mesh points are moving along with the material point and in the Eulerian description, the mesh points are fixed in space which allows large material distortion. In the third figure, arbitrary Lagrangian Eulerian description is shown where mesh points have some velocity though this need not be equal to material velocity. This mesh velocity can be imposed arbitrarily at different points in the domain.

The problem of solving the equations in a time dependent geometrical domain, while capturing the fluid-solid interfaces involved in this thesis, can be effectively handled by defining the equations in arbitrary Lagrangian Eulerian kinematics [19, 25-26]. The freedom of allocating arbitrary mesh velocity in ALE kinematics allows handling large material velocity while the Lagrangian interface tracking helps to get a clear picture of the moving particle.

3.5 Arbitrary Lagrangian Eulerian Kinematics

The Lagrangian kinematical description follows each individual particle and uses the material points as a reference domain, while the Eulerian description uses spatial points as the reference domain. Here, the material domain i.e. the Lagrangian domain of reference is denoted by R_X , made up of material particles X and the spatial domain i.e. the Eulerian domain of reference is denoted by R_x , consisting of spatial points x. As discussed in the previous section, in arbitrary Lagrangian Eulerian description neither of this material domain or spatial domain is taken as the reference. A third domain is introduced, the referential configuration R_χ where coordinates χ are used to identify the grid points. These three domains are related to each other by three conformal mappings φ, ϕ and ψ which is shown in the following figure:

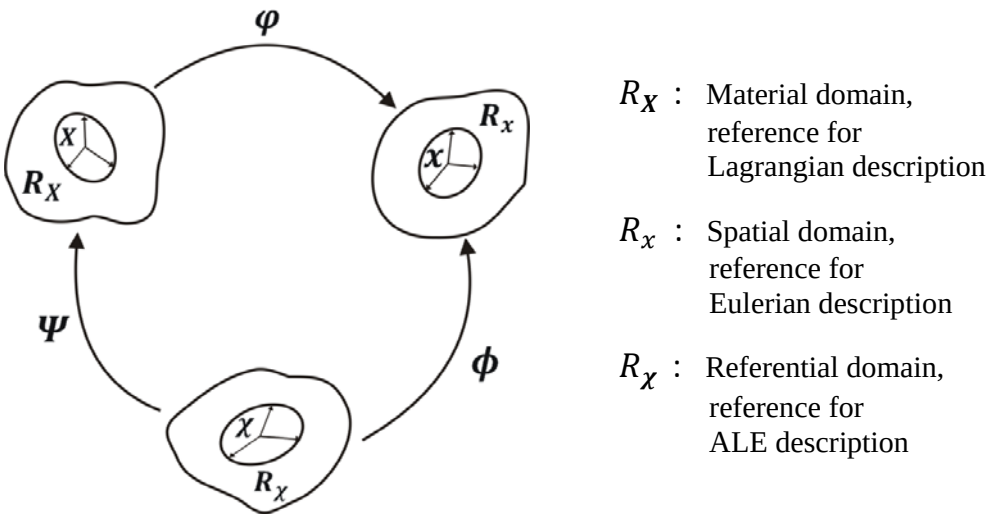

Fig. 3.3: Different reference domains and the associated mappings relating those.

The referential domain R_χ is mapped into the material and spatial domains by ψ and ϕ, respectively. The mapping φ defines the relationship between the spatial domain and material domain and can be viewed as the motion of material points. This is associated with the Lagrangian description. The mapping ϕ from the referential domain to the spatial domain can be understood as the motion of the grid points in the spatial domain. The mapping ψ defines the relationship between the referential domain and the material domain and by varying the definition of this mapping both the Eulerian and

Lagrangian description can be achieved. These three mappings are related to each other as:

$$\varphi = \phi * \psi^{-1} \tag{3.16}$$

A detail description of these three mappings along with the resulting change in the Navier-Stokes equation due to the arbitrary Lagrangian Eulerian kinematics is delineated in Appendix A. The Navier-Stokes equation and the continuity equation in arbitrary Lagrangian Eulerian description are expressed as:

$$\rho\left(\left.\frac{\delta \boldsymbol{u}}{\delta t}\right|_{\chi} + (\boldsymbol{v} - \boldsymbol{\psi_m}) \cdot \nabla \boldsymbol{u}\right) = -\nabla p + \mu \nabla \cdot (\nabla \boldsymbol{u} + \nabla \boldsymbol{u}^T) + \boldsymbol{F}_b, \tag{3.17}$$

$$\nabla \cdot \boldsymbol{u} = 0 \tag{3.18}$$

here, $\boldsymbol{\psi_m}$ is the mesh velocity. It should be noted that, the equation is similar to the Eulerian equations and can be solved in a similar way in the referential domain.

3.6 Mesh Updating Method

For computer implementation of the ALE method a mesh update procedure is necessary which will assign mesh-node velocities and displacements after each time step. When the velocity of a boundary is known a priori it is assigned to that boundary and far away from that moving boundary, mesh velocity is assigned zero. So, Lagrangian description is assigned at the moving boundary and Eulerian description is assigned far away from it. In between there is a transition region where arbitrary mesh velocity need to be defined. In this thesis, Laplacian mesh smoothing method is used for rezoning of mesh nodes in this transition region. A Laplace equation is solved to get the arbitrary mesh velocities and displacements. The elliptic mesh smoothing equation used in this analysis is:

$$\nabla^2 \boldsymbol{\psi_m} = 0 \tag{3.19}$$

This equation is solved for all the mesh velocity and displacement components.

3.7 Non-Dimensionalization of the Equations

The Navier-Stokes equation, Continuity equation and the mesh smoothing equations have been non-dimensionalized with respect to viscous time scale, $\mu/\rho a^2$. Details of the scaled parameters are given in Table 3.1. Length scales are non-dimensionalized with respect to particle radius a. Same scaling parameters are used to non-dimensionalize the mesh smoothing equations. The resulting equations are given below:

$$\frac{\partial \overline{\boldsymbol{u}}}{\partial \tau} + (\overline{\boldsymbol{u}} - \overline{\boldsymbol{\psi}}_{\boldsymbol{m}}) \cdot \overline{\nabla} \overline{\boldsymbol{u}} = -\overline{\nabla} \bar{p} + \overline{\nabla} \cdot (\overline{\nabla} \overline{\boldsymbol{u}} + \overline{\nabla} \overline{\boldsymbol{u}}^T) + \overline{\boldsymbol{F}}_b \tag{3.20}$$

$$\overline{\nabla} \cdot \overline{\boldsymbol{u}} = 0 \tag{3.21}$$

$$\overline{\nabla}^2 \overline{\boldsymbol{\psi}}_{\boldsymbol{m}} = 0 \tag{3.22}$$

Here, the overbars denote non-dimensionalized quantity. Non-dimensionalized values for all variables are taken as input to solve the above non-dimensional equation. These

equations are solved to find the wall correction factors which are also non-dimensional parameter.

Table 3.1: Non-dimensional parameters used to scale the governing equations

Variable Name	Non-dimensionalized Variable	Non-dimensionalizing Parameter
Pressure	$\bar{p}$	$\frac{\rho a^2}{\mu^2} p$
Velocity	$\bar{u}$	$\frac{\rho a}{\mu} u$
Time	τ	$\frac{\mu}{\rho a^2} t$
Force	$\bar{F}_{\mathrm{b}}$	$\frac{\rho a^3}{\mu^2} F_b$
∇ operator	$\bar{\nabla}$	a∇
Radial coordinate	$\bar{\mathrm{r}}$	$\frac{r}{a}$
Axial coordinate	$\bar{\mathrm{z}}$	$\frac{z}{a}$

3.8 Newton's Second Law of Motion for Unsteady Particle Motion

In Case-III, the motion of the suspended solid particle flowing with the fluid is analyzed. Only solving the equations for fluid flow disregarding it's interaction with the solid particle is not adequate for proper description of the problem. Here, the motion of the particle is fully developed from its hydrodynamic interaction with the fluid. The particle initially moves with an unsteady velocity, and after some time attains a uniform velocity, as the net drag force acting on it vanishes with time. Newton's second law of motion is employed to capture the instantaneous particle velocity. For a non-rotating rigid particle, with translational motion Newton's second of motion can be written as:

$$m\frac{d\boldsymbol{V}}{dt} = \boldsymbol{F} = -\int_{\partial\Omega} \boldsymbol{\sigma} \cdot \mathbf{n}\ dS \tag{3.23}$$

here, m stands for the individual particle mass, $\boldsymbol{V}$ for particle velocity and $\boldsymbol{F}$ for hydrodynamic force on the particle. $\boldsymbol{F}$ can be found from the surface integral of the total stress tensor over the particle surface $\partial\Omega$.

3.9 Boundary Conditions

3.9.1 Boundary conditions for Case-I

In present model, a spherical particle is moving with a predefined uniform velocity in a stationary fluid in the x coordinate direction. To ensure no slip condition on the particle surface axial fluid velocity u is set to be equal to particle velocity Up. The mesh on the particle surface should deform with a velocity equal to particle velocity. This is handled by assigning the x component of the mesh velocity Ψ_{mx} to be equal to Up. Fluid velocity and mesh velocity on the particle surface in other coordinate directions are set to be zero. For the mesh smoothing equation mesh displacement on all boundaries need to be defined. Since, the boundaries other than the particle surface will not deform with time mesh displacement is set to be zero on those.

For Navier Stokes equation no slip condition is applied on cylinder walls and on the walls adjacent to the reservoir. Slip condition is applied to the reservoir walls. At inlet of the reservoir a zero velocity condition is employed and the outlet of the fluid receiving reservoir is set to be a zero total stress condition. This is illustrated in Figure 3.4. In Table 3.2, the mathematical form of the applied boundary conditions are given.

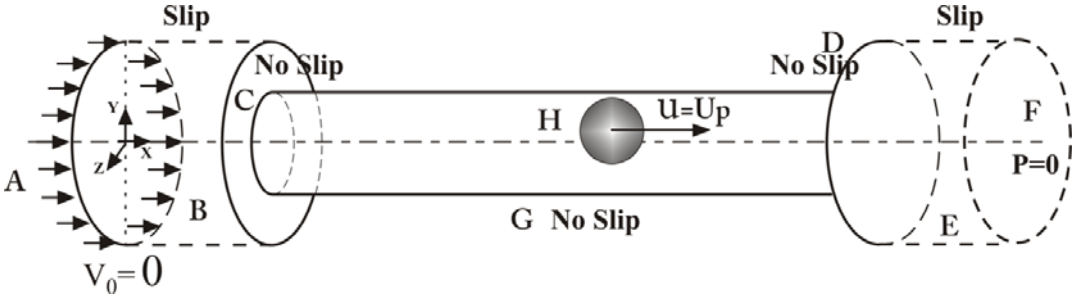

(a) Navier-Stokes equation

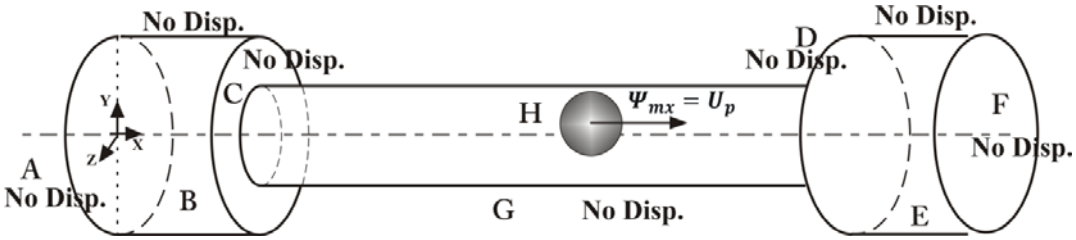

(b) Mesh smoothing equation

Fig. 3.4: Boundary conditions for Case-I (a) Navier Stokes module (b) Mesh smoothing equation

Table 3.2: Boundary conditions for Case-I

Boundaries	Boundary Type		
	Incompressible Navier Stokes Equation		Mesh Velocity
Cylinder Wall	No Slip	$\vec{\boldsymbol{u}} = 0$	No Disp.
Particle Surface	Velocity	$u = U_p, v = 0, w = 0$	$\Psi_{mx} = U_p,$ $\Psi_{my} = \Psi_{mz} = 0$
Wall Adjacent to Reservoir	No Slip	$\vec{\boldsymbol{u}} = 0$	No Disp.
Reservoir Wall	Slip	$\boldsymbol{n} \cdot \vec{\boldsymbol{u}} = 0$ $\boldsymbol{t} \cdot \left[-p\bar{\bar{\boldsymbol{I}}} + \mu(\nabla \boldsymbol{u} + (\nabla \boldsymbol{u})^T)\right]\boldsymbol{n} = 0$	No Disp.
Reservoir Inlet	Velocity	$\vec{\boldsymbol{u}} = 0$	No Disp.
Reservoir Outlet	Zero Total Stress	$\left[-p\bar{\bar{\boldsymbol{I}}} + \mu(\nabla \boldsymbol{u} + (\nabla \boldsymbol{u})^T)\right]\boldsymbol{n} = 0$	No Disp.

3.9.2 Boundary conditions for Case-II

In Case-II scenario, the particle is set to be fixed at a point. The computational mesh is not deforming with time and boundary conditions are only applied for the Navier-Stokes equation. A Poiseuille flow is produced inside the cylinder. At reservoir inlet a uniform inflow velocity is applied and the outlet of the fluid receiving reservoir is set to the zero total stress condition. All the other boundaries are set as no slip condition, except at the reservoir wall where slip condition is employed. These are illustrated in Figure 3.5 below. In Table 3.3, the applied boundary conditions are summarized.

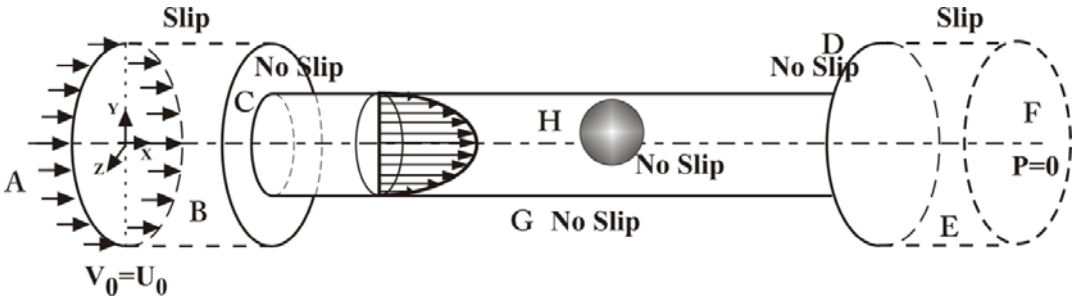

Fig. 3.5: Boundary conditions for Case-II

Table 3.3: Boundary conditions for Case-II

Boundaries	Boundary Type	
Channel Wall	No Slip	$\vec{\boldsymbol{u}} = 0$
Particle Surface	No Slip	$\vec{\boldsymbol{u}} = 0$
Wall Adjacent to Reservoir	No Slip	$\vec{\boldsymbol{u}} = 0$
Reservoir Wall	Slip	$\boldsymbol{n} \cdot \vec{\boldsymbol{u}} = 0$ $\boldsymbol{t} \cdot \left[-p\bar{\bar{\boldsymbol{I}}} + \mu(\nabla \boldsymbol{u} + (\nabla \boldsymbol{u})^T)\right]\boldsymbol{n} = 0$
Reservoir Inlet	Normal Inflow Velocity	$\vec{\boldsymbol{u}} = -U_o \boldsymbol{n}$
Reservoir Outlet	Zero Total Stress	$\left[-p\bar{\bar{\boldsymbol{I}}} + \mu(\nabla \boldsymbol{u} + (\nabla \boldsymbol{u})^T)\right]\boldsymbol{n} = 0$

3.9.3 Boundary conditions for Case-III

The boundary conditions for Case-III are same as that of Case-I. However, as the particle velocity U_p is not known a priori, the fluid velocity in the x direction and the mesh velocity in the same direction on the particle surface are found from solving an ordinary differential equation (Eq. 3.23). The dependent variable of this equation is applied to be equal to u and Ψ_{mx} as the boundary condition. In Table 3.4, the applied boundary conditions are summarized.

Table 3.4: Boundary conditions for Case-III

Boundaries	Boundary Type		
	Incompressible Navier Stokes Equation		Mesh Velocity
Cylinder Wall	No Slip	$\vec{\boldsymbol{u}} = 0$	No Disp.
Particle Surface	Velocity	$u = U_p, v = 0, w = 0$	$\Psi_{mx} = U_p,$ $\Psi_{my} = \Psi_{mz} = 0$
Wall Adjacent to Reservoir	No Slip	$\vec{\boldsymbol{u}} = 0$	No Disp.
Reservoir Wall	Slip	$\boldsymbol{n} \cdot \vec{\boldsymbol{u}} = 0$ $\boldsymbol{t} \cdot \left[-p\bar{\bar{\boldsymbol{I}}} + \mu(\nabla \boldsymbol{u} + (\nabla \boldsymbol{u})^T)\right]\boldsymbol{n} = 0$	No Disp.
Reservoir Inlet	Velocity	$\vec{\boldsymbol{u}} = 0$	No Disp.
Reservoir Outlet	Zero Total Stress	$\left[-p\bar{\bar{\boldsymbol{I}}} + \mu(\nabla \boldsymbol{u} + (\nabla \boldsymbol{u})^T)\right]\boldsymbol{n} = 0$	No Disp.

4. NUMERICAL SOLUTION METHODOLOGY

4.1 Finite Element Method

Finite element method (FEM) is employed for solving the governing equations. The method is well described in literature [27-28] and is widely used for solving differential equations in many areas of engineering and science. In finite element method, the computational domain is approximated as a piecewise combination of small interconnected domains. This involves discretizing the problem geometry to finite number of elements. This process is called mesh generation. The responses of the dependent variables are assumed a priori. State variables are approximated by discretely describable functions. These functions are called shape functions or basis functions, which are formulated from simple functions like polynomials, based on the discretization of the problem geometry. Approximating piecewise function for state variables are called test functions. Then variational principle, the Galerkin method is applied to find the weak form of the governing equations. The dependent variables in this weak form are replaced by their corresponding discrete form i.e the test functions. Replacing the shape function in the discretized weak equations by the shape functions associated to each computational node gives a single algebraic equation which satisfies the discretized form of the governing equations. In this way a system of algebraic equations are formed. These equations describe the relationship between the coefficients of the test functions. Solving these algebraic equations for these coefficients the behavior of the dependent variable is obtained.

Here, the weak form of the governing equations that are formulated in the previous chapter is derived.

4.1.1 Weak form of Navier-Stokes equation in ALE kinematics

Neglecting the body force and using the total stress tensor notation the Navier-Stokes equation in arbitrary Lagrangian Eulerian framework takes this form:

$$\frac{\delta u}{\delta t} + (u - \psi_m).\nabla u - \nabla.\sigma_{ij} = 0 \tag{4.1}$$

Considering momentum conservation in three space directions three different equations can be obtained. Using Einstein summation convention, which implies summation over repeated index the Navier-Stokes equation is written as:

$$\frac{\delta u_i}{\delta t} + \left(u_j - \psi_{mj}\right)\delta_j u_i - \delta_j \sigma_{ij} = 0\,, \tag{4.2}$$

here i denotes the coordinate direction for momentum conservation. So, u_i denotes the velocity component in i^{th} space direction. It is important to note here that, the equations are needed to be solved in a time dependent domain, which is denoted as the deformed frame $\overline{\Omega}$ having coordinate dimensions x, y and z. So, to get the weak form of this

equation it is multiplied by the basis function for velocity and integrated over the whole subdomain $\overline{\Omega}$. This is the well known Petrov-Galerkin discretization method. Here, the basis function or the test function of the ith component of the velocity u_i is denoted as $\widehat{u_i}$. So, the weak form can be written as:

$$\int_{\overline{\Omega}} \widehat{u_i} \left\{ \frac{\delta u_i}{\delta t} + \left(u_j - \psi_{mj}\right)\delta_j u_i - \delta_j \sigma_{ij} \right\} \mathrm{d}\overline{\Omega} = 0$$

$$\Rightarrow \int_{\overline{\Omega}} \widehat{u_i} \, \frac{\delta u_i}{\delta t} \mathrm{d}\overline{\Omega} + \int_{\overline{\Omega}} \widehat{u_i}\left(u_j - \psi_{mj}\right)\delta_j u_i \mathrm{d}\overline{\Omega} - \int_{\overline{\Omega}} \widehat{u_i}\delta_j \sigma_{ij} \mathrm{d}\overline{\Omega} = 0 \tag{4.3}$$

Now, the order of differentiation in the third term is reduced by using the integration by parts rule.

$$\int_{\overline{\Omega}} \widehat{u_i}\delta_j \sigma_{ij} \mathrm{d}\overline{\Omega}$$

$$= \widehat{u_i} \int_{\overline{\Omega}} \delta_j \sigma_{ij} \mathrm{d}\overline{\Omega} - \int_{\overline{\Omega}} (\delta_j \widehat{u_i})\sigma_{ij} \mathrm{d}\overline{\Omega}$$

$$= \int_{\delta\overline{\Omega}} \widehat{u_i}\sigma_{ij} \mathrm{ds} - \int_{\overline{\Omega}} (\delta_j \widehat{u_i})\sigma_{ij} \mathrm{d}\overline{\Omega} \tag{4.4}$$

The first term in Equation (4.4) denotes integration over the boundary $\delta\overline{\Omega}$. This term is the natural boundary condition and should be satisfied by choosing appropriate basis function. It is taken care of by the applied boundary conditions.

So, the weak form of the Navier-Stokes equation without the boundary integrals takes the following form:

$$\int_{\overline{\Omega}} \widehat{u_i} \, \frac{\delta u_i}{\delta t} \mathrm{d}\overline{\Omega} + \int_{\overline{\Omega}} \widehat{u_i}\left(u_j - \psi_{mj}\right)\delta_j u_i \mathrm{d}\overline{\Omega} + \int_{\overline{\Omega}} (\delta_j \widehat{u_i})\sigma_{ij} \mathrm{d}\overline{\Omega} = 0 \tag{4.5}$$

From this, one can easily find three weak equations for three coordinate directions. Here, by taking i = 1 the equation denoting momentum conservation in the x coordinate direction is written. Since, Einstein summation convention is used the value of the repeating index j is taken to be 1, 2 and 3 representing three space dimensions. The resulting equation is as follows:

$$\int_{\overline{\Omega}} \Big\{ \widehat{u_1} \, \frac{\delta u_1}{\delta t} + \widehat{u_1}(u_1 - \psi_{m1})\delta_1 u_1 + \widehat{u_1}(u_2 - \psi_{m2})\delta_2 u_1 + \widehat{u_1}(u_3 - \psi_{m3})\delta_3 u_1 + \delta_1 \widehat{u_1}\sigma_{11} + \delta_2 \widehat{u_1}\sigma_{12} + \delta_3 \widehat{u_1}\sigma_{13} \Big\} \delta\overline{\Omega} = 0 \tag{4.6}$$

Now, the following are replaced in the above equation:

$$u_1 = u, u_2 = v, u_3 = w, \widehat{u_1} = \hat{u}, \delta_1 = \frac{\delta}{\delta x}, \delta_2 = \frac{\delta}{\delta y}, \delta_3 = \frac{\delta}{\delta z},$$

$$\sigma_{11} = \sigma_{xx}\,, \sigma_{12} = \sigma_{xy}\;\; \sigma_{13} = \sigma_{xz}\,,$$

$$\psi_{m1} = \psi_{mx}\,, \psi_{m2} = \psi_{my}\,, \psi_{m3} = \psi_{mz} \tag{4.7}$$

to get the equation presented below:

$$\int_{\bar{\Omega}} \left\{ \hat{u}\,\frac{\delta u}{\delta t} + \hat{u}(u - \psi_{mx})\frac{\delta u}{\delta x} + \hat{u}\big(v - \psi_{my}\big)\frac{\delta u}{\delta y} + \hat{u}(w - \psi_{mz})\frac{\delta u}{\delta z} + \frac{\delta \hat{u}}{\delta x}\sigma_{xx} + \frac{\delta \hat{u}}{\delta y}\sigma_{xy} + \frac{\delta \hat{u}}{\delta z}\sigma_{xz} \right\} \delta\bar{\Omega} = 0 \tag{4.8}$$

Here, u, v and w are the fluid velocity components and $\psi_{mx}\,, \psi_{my}$ and ψ_{mz} are the mesh velocity components in the x, y and z coordinate direction respectively. The values of σ_{xx}, σ_{xy} and σ_{xz} can be expressed in terms of velocity gradient, kinematic viscosity υ and pressure. The above equation can be written as:

$$\int_{\bar{\Omega}} \left\{ \hat{u}\,\frac{\delta u}{\delta t} + \hat{u}(u - \psi_{mx})\frac{\delta u}{\delta x} + \hat{u}\big(v - \psi_{my}\big)\frac{\delta u}{\delta y} + \hat{u}(w - \psi_{mz})\frac{\delta u}{\delta z} + \frac{\delta \hat{u}}{\delta x}(2\upsilon\frac{\delta u}{\delta x} - p) + \frac{\delta \hat{u}}{\delta y}\upsilon\left(\frac{\delta u}{\delta y} + \frac{\delta v}{\delta x}\right) + \frac{\delta \hat{u}}{\delta z}\upsilon\left(\frac{\delta u}{\delta z} + \frac{\delta w}{\delta x}\right) \right\} \delta\bar{\Omega} = 0 \tag{4.9}$$

4.1.2 Weak form of the Continuity equation

The weak form of the continuity equation is found by multiplying it by the pressure basis function and integrating over the whole subdomain (in deformed frame $\bar{\Omega}$). Here the basis function or test function for pressure is denoted as $\hat{p}$. So the weak form of continuity equation becomes:

$$\int_{d\bar{\Omega}} \{\hat{p}(\nabla . u)\}\delta\bar{\Omega} = 0$$

$$\Rightarrow \int_{\bar{\Omega}} \left\{ \hat{p}\left(\frac{\delta u}{\delta x} + \frac{\delta v}{\delta y} + \frac{\delta w}{\delta z}\right) \right\} \delta\bar{\Omega} = 0 \tag{4.10}$$

4.1.3 Weak form of the elliptic mesh smoothing equation

The elliptic mesh smoothing equation that have been used is as follows:

$$\nabla^2 \psi_m = 0, \tag{4.11}$$

here,

$$\psi_m = \frac{\delta x_i}{\delta t} \tag{4.12}$$

and, x_i denotes the deformed mesh coordinate in the i^{th} coordinate direction i.e. it could be x, y or z. So the elliptic equation can be written as:

$$\nabla^2 \frac{\delta x_i}{\delta t} = 0 \tag{4.13}$$

One point to note here that, it is needed to find the mesh deformation at each node point in the geometrical domain, which is denoted as reference frame Ω. So, the above equation is solved in this fixed frame Ω. To find the weak form of this differential equation, it is multiplied by the basis function of x_i, which is denoted by $\hat{x}_i$ and integrated over the reference frame Ω where the coordinate of each point is denoted by X, Y and Z.

So the resulting equation is:

$$\int_{\Omega} \left\{ \hat{x}_i \, \nabla^2 \frac{\delta x_i}{\delta t} \right\} d\Omega = 0 \tag{4.14}$$

Now, the integration by parts rule is applied to reduce the order of differentiation in the above equation, which results:

$$\hat{x}_i \int_{\Omega} \nabla^2 \frac{\delta x_i}{\delta t} \, d\Omega - \int_{\Omega} \nabla \hat{x}_i . \left(\int_{\Omega} \nabla^2 \frac{\delta x_i}{\delta t} d\Omega \right) d\Omega = 0$$

$$\Longrightarrow \int_{\partial\Omega} \hat{x}_i \left(\nabla \frac{\delta x_i}{\delta t} \right) . n \, ds - \int_{\Omega} \nabla \hat{x}_i . \nabla \frac{\delta x_i}{\delta t} \, d\Omega = 0 \tag{4.15}$$

The first boundary integral term is specified through the given boundary conditions, so the final equation becomes:

$$\int_{\Omega} \nabla \hat{x}_i . \nabla \frac{\delta x_i}{\delta t} \, d\Omega = 0 \tag{4.16}$$

The equation for x component of mesh displacements or velocity can be found by placing i =1.

$$\int_{\Omega} \nabla x . \nabla \frac{\delta x}{\delta t} \, d\Omega = 0$$

This can be written in detail as:

$$\Longrightarrow \int_{\Omega} \left\{ \frac{\delta \hat{x}}{\delta X} \left(\frac{\delta}{\delta X} \frac{\delta x}{\delta t} \right) + \frac{\delta \hat{x}}{\delta Y} \left(\frac{\delta}{\delta Y} \frac{\delta x}{\delta t} \right) + \frac{\delta \hat{x}}{\delta Z} \left(\frac{\delta}{\delta Z} \frac{\delta x}{\delta t} \right) \right\} d\Omega = 0 \tag{4.17}$$

4.2 Computer Implementation

In the previous description of arbitrary Lagrangian Eulerian viewpoint, it is described that, Navier-Stokes and continuity equations are solved in a time dependent domain and the mesh smoothing equations are solved in a fixed geometrical domain. Two frames of references are introduced. One is the fixed domain $\Omega\,(X, Y, Z)$ which is called the reference frame and the other frame $\overline{\Omega}\,(x, y, z)$ is the time dependent domain. As $\overline{\Omega}\,(x, y, z)$ is deforming with time it is termed as the deformed frame. The elliptic mesh smoothing equations along with the specified boundary conditions defines the mapping between the reference frame and the deformed frame i.e. the coordinate transformation between (x, y, z) and (X, Y, Z).

4.2.1 Mesh generation

In this analysis the three dimensional problem geometry is discretized by tetrahedral elements. The surfaces are discretized by triangular elements. Higher number of mesh elements is used on the spherical particle surface. This facilitates capturing the higher velocity gradient near the particle surface arising from the no slip boundary condition. To find the force on the particle total stress tensor is integrated over the particle surface. This local higher mesh density ensures the accuracy of this integration.

4.2.2 Shape functions or basis functions

Second order quadratic Lagrangian shape functions are used to approximate velocity function and first order linear Lagrangian shape functions are used to approximate the pressure function.

4.2.3 Gauss quadrature integration order

To implement the integrals arising from the discretized weak form of Navier-Stokes and other equations Gauss quadrature rule need to be implemented. In this analysis 4^{th} order Gauss quadrature integration technique is used for all integrations.

4.2.4 Algebraic equations solving technique

For models with many dependent variables direct solver needs a huge memory. So, a memory efficient iterative solver GMRES (Generalized Minimum Residual) is used to solve the resulting matrix equations. Unlike direct solvers iterative solvers does not converge easily. To improve the convergence of the iterative solver a precondtioner named, incomplete LU, that performs an incomplete LU factorization of the system matrix A, is used. Thus, it saves memory and the resulting factors L and U are approximation to A. An optimum value of drop tolerance is used for the LU preconditioner. A high value of drop tolerance minimizes memory requirement, however, it causes inaccuracy in the LU factorization, which as a result affects the

convergence of the iterative solver. So, the maximum value of drop tolerance that ensures convergence is selected.

4.2.5 Computer configuration

Intel Core i5 processor and 4GB RAM are employed to obtain the solutions presented here.

4.3 Implementation of Case-III

The whole procedure in Case-III is same as Case-I, except that here the particle velocity U_p is not prescribed a priori, but determined by solving Equation (3.23). It is implemented by coupling an ordinary differential equation with the governing partial differential equations such as, Navier-Stokes and mesh smoothing equations. The right hand side boundary integration term in Equation (3.23) is implemented by defining an integration coupling variable with global destination. The value of this integration coupling variable is the integration of total stress tensor over the particle surface and is available during the simulation as global variable. The mass of the spherical particle is defined to be equal to that of the fluid as neutrally buoyant particle is considered in the analysis. The dependent variable of the Equation (3.23) is the particle velocity and its value is given as U_p in the boundary condition for Navier-Stokes and mesh smoothing equations.

4.4 Mesh Sensitivity Analysis

The mesh sensitivity analysis is performed for both Case-I and Case-II by observing the improvement in the calculated values of wall correction factors K_1 and K_2, respectively, with increasing number of mesh elements. A spherical particle having particle to channel radii ratio 0.5 is taken. In both cases of this analysis the particle lies along the axis of the cylinder. Tests are performed from nearly 5000 elements to 30000 elements in Case-I and up to 50000 elements in Case-II. Since, in Case-I, the problem is time dependent, memory requirement for computation is higher than the stationary problem, i.e. the Case-II. Moreover, in Case-I, three mesh smoothing equations are coupled with the Navier-Stokes and continuity equation, which increases the number of degrees of freedom for each mesh node. This means, at each node three additional mesh displacement variables (x, y and z) are solved with the dependent variables of Navier-Stokes equation (u, v, w and p). For this reason, number of mesh elements for Case-I, is taken lower than that of Case-II to minimize the memory and time requirement.

Values of wall correction factor K_1 for different number of mesh elements is shown in Fig. 4.1. It is well noticeable that, the value of K_1 for this specific case cannot be improved significantly by taking higher number of elements above 20000. However, in this analysis the model is solved for different eccentric positions of the sphere. The separation between the particle and channel wall is significantly reduced at higher values of eccentricity. This narrow region in geometry requires more mesh elements to

capture the sharp velocity gradient developed in that region. To ensure computational accuracy, more than 30000 elements are taken when the separation between the particle and channel wall is reduced. Another point should be noted that, computations containing smaller λ values require more mesh elements as the computational domain gets bigger. Moreover, to maintain comparatively higher mesh density on the particle surface than that in the other regions inside the computational domain, the total number of mesh elements increases as the particle size is decreased while the size of the computational domain remains the same. So, for Case-I, mesh elements are taken in between 20000 to 45000 considering the above mentioned factors.

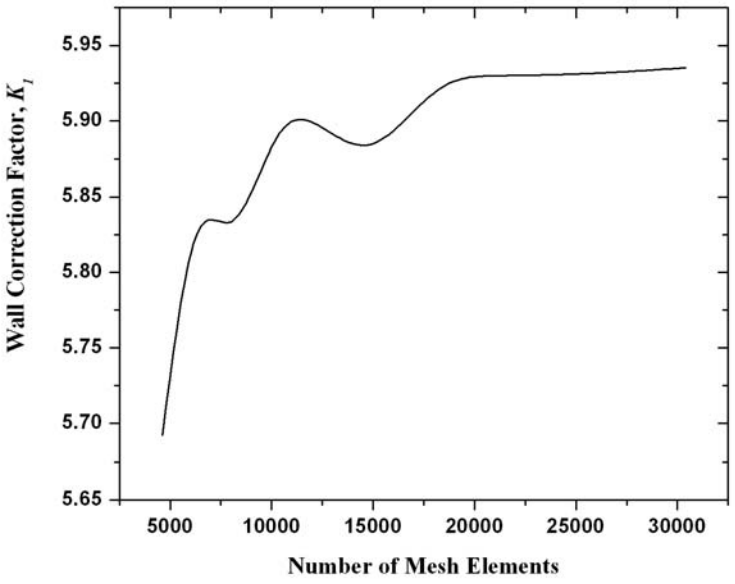

Figure 4.1: Mesh sensitivity analysis for wall correction factor, K_1

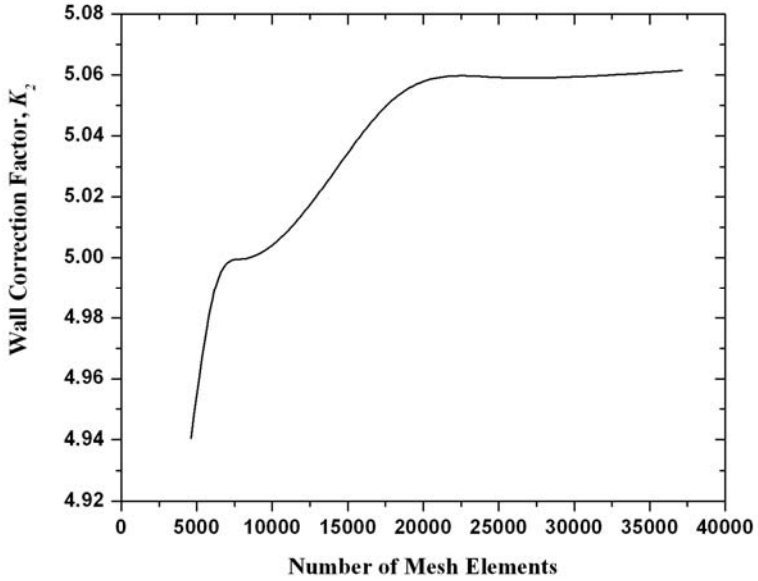

Figure 4.2: Mesh sensitivity analysis for wall correction factor, K_2

Variation of wall correction factor K_2 with the number of mesh elements is shown in Figure 4.2. It can be observed that, for this specific analysis number of mesh elements more than 20000 can be used to get the mesh insensitive result. However, in all the analysis around 50000 elements are taken to take into account of the eccentricity of the particle and the smaller particle size.

4.5 Flowchart of the Overall Solution Methodology

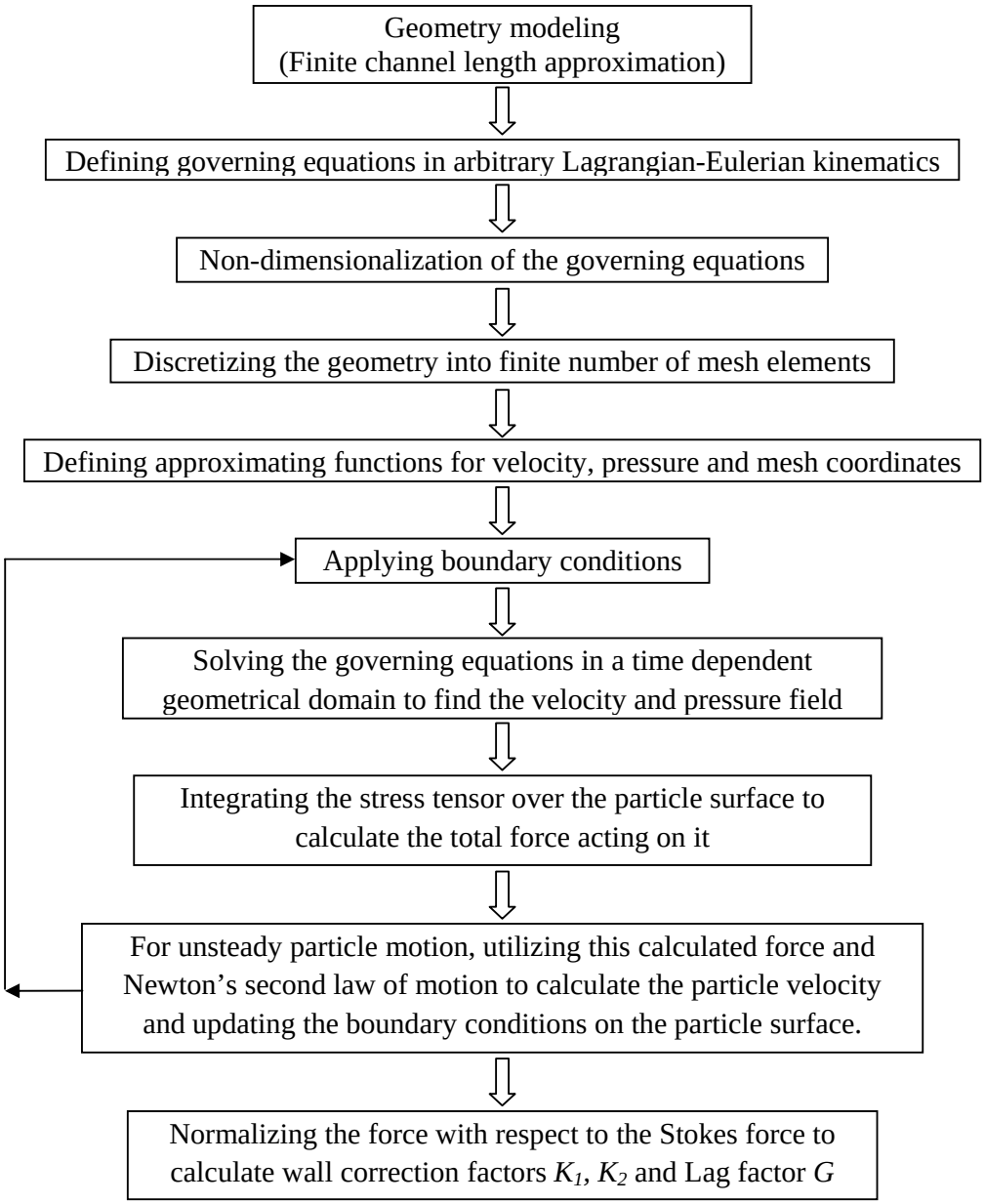

5. RESULT AND DISCUSSION

This chapter provides the wall correction factors and lag factor for a spherical particle flowing parallel to the channel axis at different radial positions. The developed model utilized in this analysis, is validated by comparing the calculated values of wall correction factors and lag factor for the centerline motion of the spherical particle, with those available in the literature. Later, wall correction factors and lag factor are presented for a spherical particle of different sizes, covering the range of particle to channel radii ratio, $0.2 \leq \lambda \leq 0.9$ and of different radial positions, covering the eccentricity value in the range of $0 \leq e \leq 0.8$.

5.1 Model Validation

Values of wall correction factor K_1 and K_2 for the centerline motion of the sphere for different λ values are calculated utilizing the developed model namely, NS-ALE model. These calculated values are compared with the published analytically and numerically computed results. An exact theoretical solution for the wall correction factors for the centerline motion is available in terms of an infinite set of linear algebraic equations for the coefficients of Stokes stream functions [11]. Very accurate values of wall correction factors for all λ values were provided using singular perturbation techniques [5]. Values of wall correction factors were calculated by using spectral boundary element method, which further validated the previously provided results [6]. The latest investigation of this problem was done utilizing the finite difference method [17]. In Table 5.1 and 5.2, the calculated values of wall correction factors K_1 and K_2 from the NS-ALE model is presented in tabular form, along with the values found from the above mentioned theoretical and numerical investigations. It is well noticeable that the values calculated by the NS-ALE model are indistinguishable with the other results.

The percentage of error for the values of calculated wall correction factor K_1 when compared to the values of [5] for λ = 0.2 and λ = 0.8 are 0.519 % and 0.149 %, respectively. The percentage of error in K_2 for λ = 0.2 and λ = 0.8 are 0.47 % and 0.201 %, respectively. A graphical comparison for the values of wall correction factor K_1 and K_2 presented in Table 5.1 and Table 5.2 is shown in Fig. 5.1. In Fig. 5.2, the calculated values of lag factor, $G\ (= \frac{K_2}{K_1})$ is compared with the other results. These two graphs also reveal the accuracy of the presented NS-ALE model.

Table 5.1: Comparison of wall correction factor K_1

$\lambda = a/r_0$	Values of wall correction factor, K_1				
	NS-ALE	Haberman & Sayre [11]	Bungay & Brenner [5]	Higdon & Muldowney [6]	Ben Richou [17]
0.1	1.2621	1.263	1.2632	1.2632	1.2764
0.2	1.67088	1.68	1.6796	1.6794	1.6927
0.3	2.3502	2.371	2.3707	2.37	2.3824
0.4	3.57253	3.596	3.5938	3.5913	3.6058
0.5	5.92496	5.97	5.9548	5.9473	5.9638
0.6	11.03425	11.135	11.1099	11.0918	11.1136
0.7	24.52592	24.955	24.7144	24.6759	24.6932
0.8	74.63405	73.555	74.7459	74.6698	74.6191
0.9	469.1	-	469.3734	469.2225	468.2021

Table 5.2: Comparison of wall correction factor K_2

$\lambda = a/r_0$	Values of wall correction factor, K_2				
	NS-ALE	Haberman & Sayre [11]	Bungay & Brenner [5]	Higdon & Muldowney [6]	Ben Richou [17]
0.1	1.23943	1.255	1.2548	1.2547	1.2691
0.2	1.62681	1.635	1.6345	1.6347	1.6488
0.3	2.21656	2.231	2.2285	2.2289	2.2428
0.4	3.20685	3.218	3.216	3.2157	3.2332
0.5	4.9837	5.004	4.9992	4.9953	5.0245
0.6	8.59728	8.651	8.6255	8.613	8.6413
0.7	17.45599	17.671	17.5029	17.474	14.512
0.8	47.58021	43.301	47.6762	47.6201	47.6288
0.9	267.0977	-	266.5299	266.432	265.9404

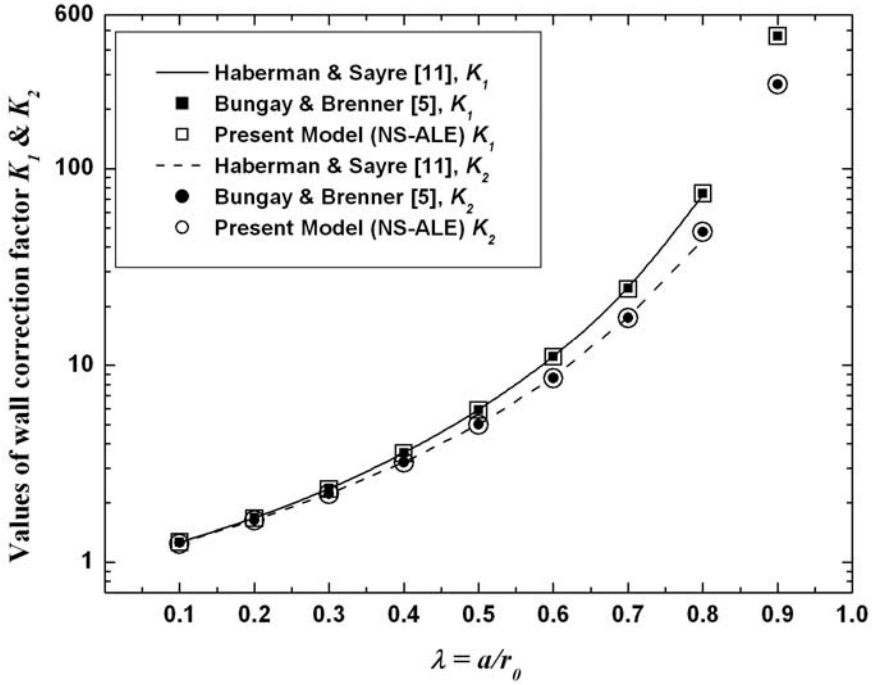

Figure 5.1: Comparison of wall correction factor, K_1 and K_2 for the centerline motion of the sphere

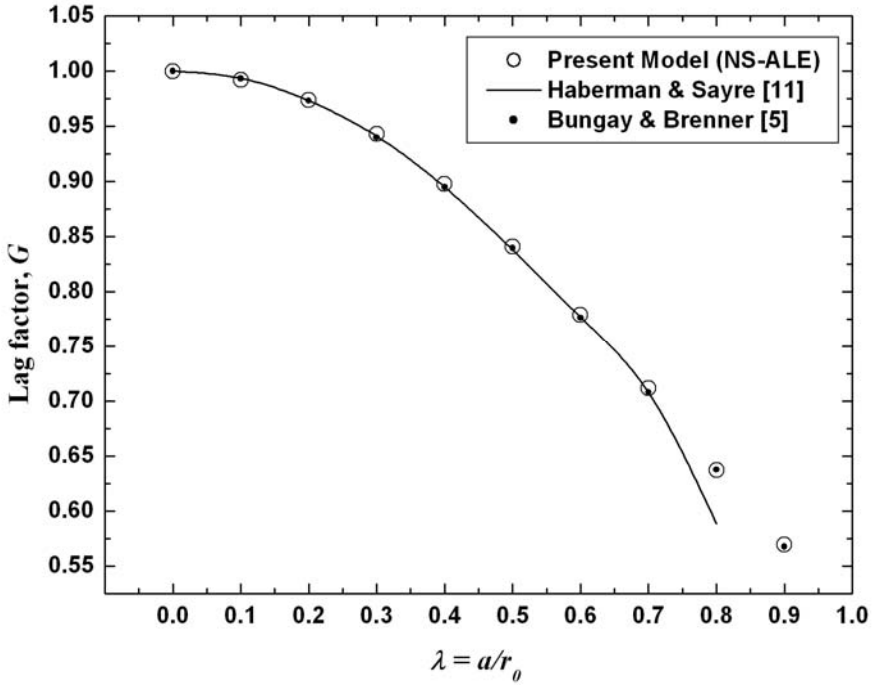

Figure 5.2: Comparison of lag factor G for the centerline motion of the sphere

5.2 Effect of Eccentricity of the Particle on its Motion

The effect of eccentricity of the particle on its motion inside the cylindrical channel is quantified in terms of the wall correction factor K_1, K_2 and lag factor G. The relative size of the particle is denoted by $\lambda\ (= a/r_0)$ and the eccentricity of the particle is denoted by $e\ (= d/(r_0 - a))$. Values of K_1, K_2 and G are calculated for each λ value within the range $0.2 \leq \lambda \leq 0.9$ considering the eccentricity of the particle to be within the range of $0 \leq e \leq 0.8$ for each λ value. Fig. 5.3 provides a graphical representation of the variation of K_1, K_2 and G with the particle's radial position inside the channel, for all these relative particle sizes.

The drag on an eccentrically positioned particle held fixed in a Poiseuille flow is characterized by the wall correction factor K_2. This value represents the ratio of the drag force on the particle inside the channel with respect to the Stokes drag in an unbounded fluid. For calculating the Stokes drag force on the eccentrically positioned particle, the local fluid velocity at that position is used. This is a rational choice, because this calculated value of K_2 is used to find the lag factor of the particle which is defined as the ratio of the particle velocity to the local undisturbed fluid velocity.

From Fig. 5.3, it is observed that, values of wall correction factor K_2 for larger sized particles ($\lambda > 0.3$) decreases monotonically with eccentricity. But for smaller sized particles ($\lambda < 0.3$), the values of K_2 initially decreases and then have a tendency to increase at eccentricity value around $e = 0.6$. Decrease of K_2 with eccentricity can be explained by the fact that, when the particle is moved to eccentric position, the gap between the particle wall and the channel wall decreases. The additional pressure drop resulting from the presence of the particle is increased due to the narrow region between the particle and channel wall. This causes the fluid velocity in the narrow region to be considerably small. This is illustrated in Figure 5.4. The figure shows the fluid velocity parallel to the channel axis at a cross section through the particle center. It can be easily noticed that the velocity in the narrow region is considerably smaller than the velocity in the wider gap between the particle and channel surface. Pressure gradient across the cross section is also shown in Figure 5.5. The smaller velocity gradient on the half of the particle surface that is facing the channel wall causes the overall viscous stress tensor on the particle surface to decrease compared to the concentric case. This results in a lower viscous drag on the particle.

For smaller particle sizes the value of K_2 initially decreases with eccentricity and start to increase at higher eccentric positions. The parabolic velocity profile accounts for this increase. For smaller sized particles at higher eccentricity values the local fluid velocity at the radial position same to the particle center is significantly lower than the centerline velocity. But for larger sized particles the radial movement of the particle center cannot be high due to the narrow available region between the channel and particle wall. So, in this case the local velocity at any eccentric position of the sphere is almost near to the centerline velocity and also higher than the mean fluid velocity within the channel. To

summarize, it can be said that, normalizing the drag with respect to the smaller local velocity for smaller particles at higher eccentricity results the increase in K_2. But, for higher particle sizes the normalizing velocity does not decrease significantly with eccentricity. This results in the monotonic decrease in K_2.

For a steadily moving particle in an otherwise quiescent fluid, the particle drag is characterized by the wall correction factor K_1. The value of K_1 also decreases because the recirculation fluid velocity within the gap between the particle and channel wall is restricted. This causes the velocity gradient to reduce on the particle surface and thus results in a lower viscous drag on the steadily moving particle near to the channel wall. The settling velocity of the particle is increased with eccentricity.

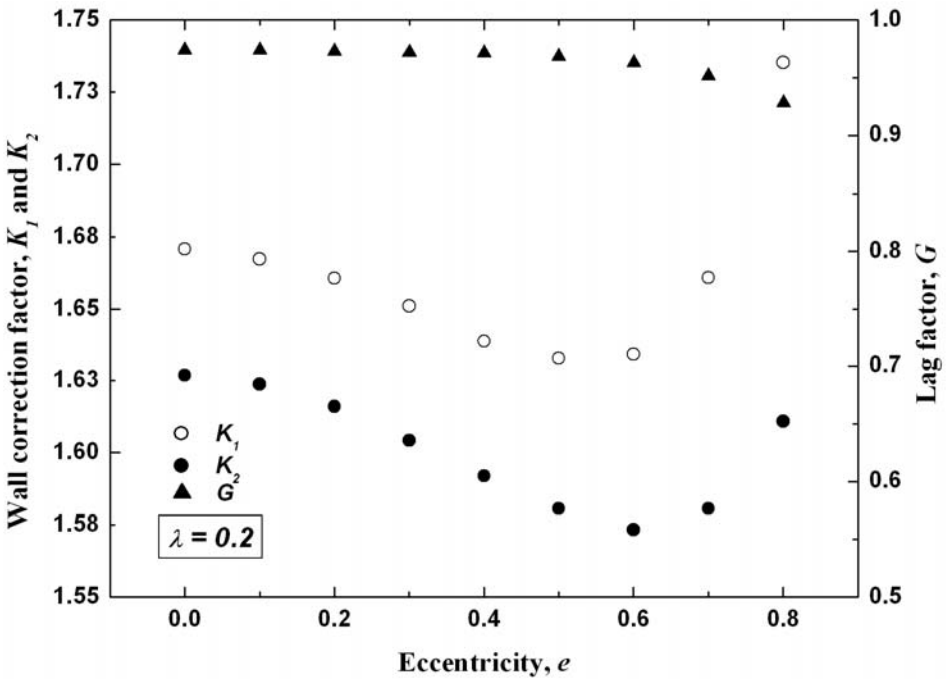

(a) Variation of wall correction factors K_1, K_2 and lag factor G for $\lambda = 0.2$

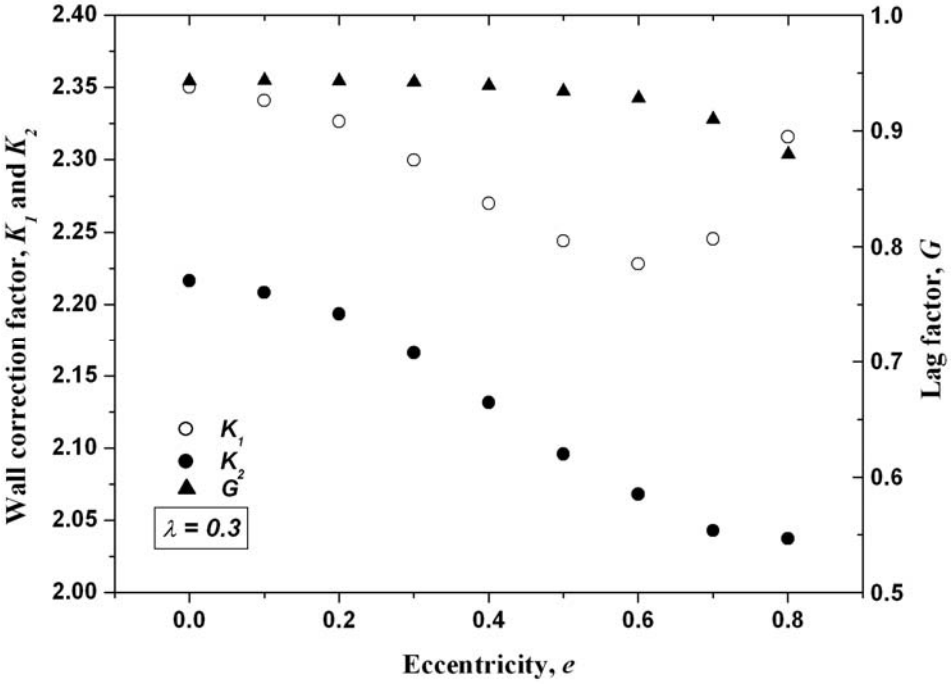

(b) Variation of wall correction factors K_1, K_2 and lag factor G for λ = 0.3

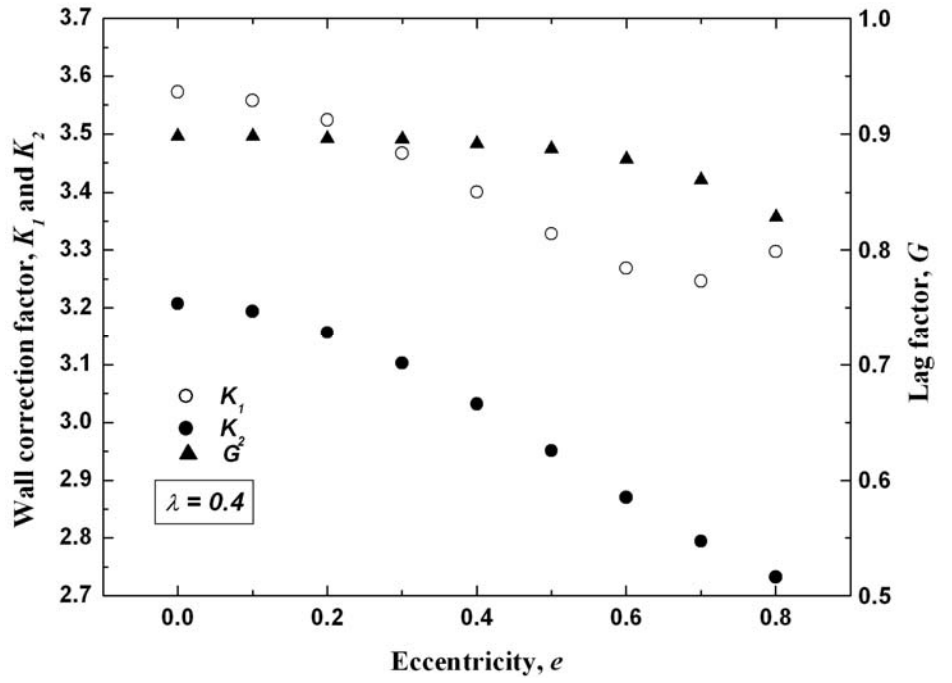

(c) Variation of wall correction factors K_1, K_2 and lag factor G for λ = 0.4

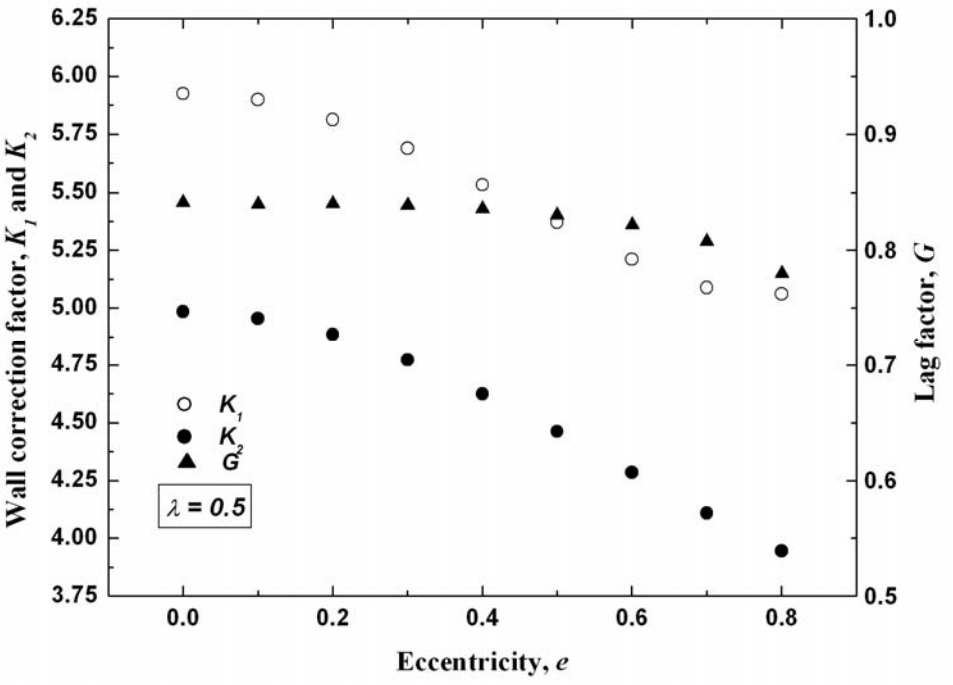

(d) Variation of wall correction factors K_1, K_2 and lag factor G for $\lambda = 0.5$

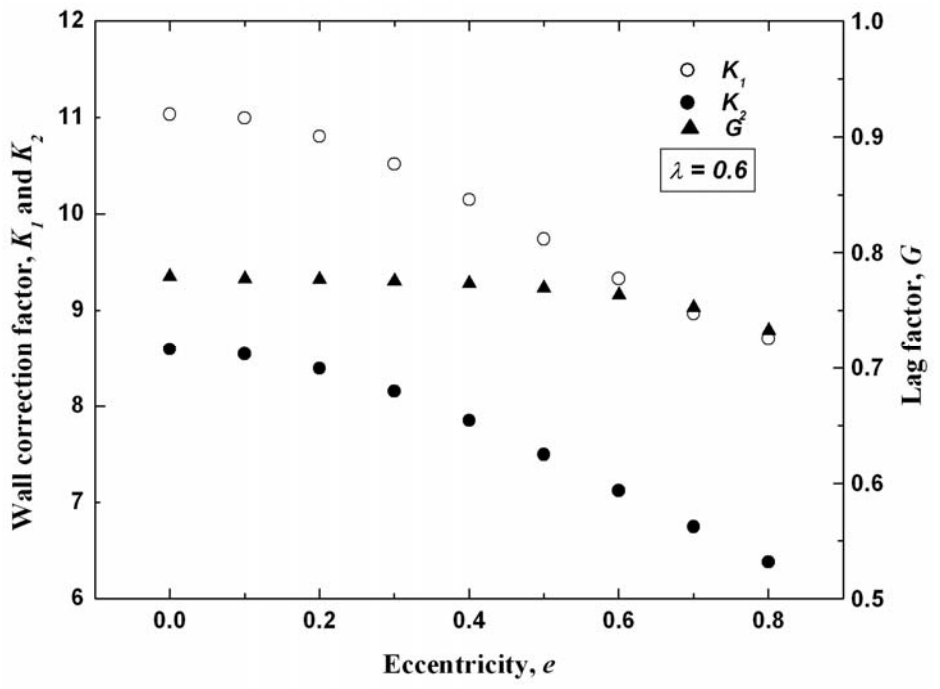

(e) Variation of wall correction factors K_1, K_2 and lag factor G for $\lambda = 0.6$

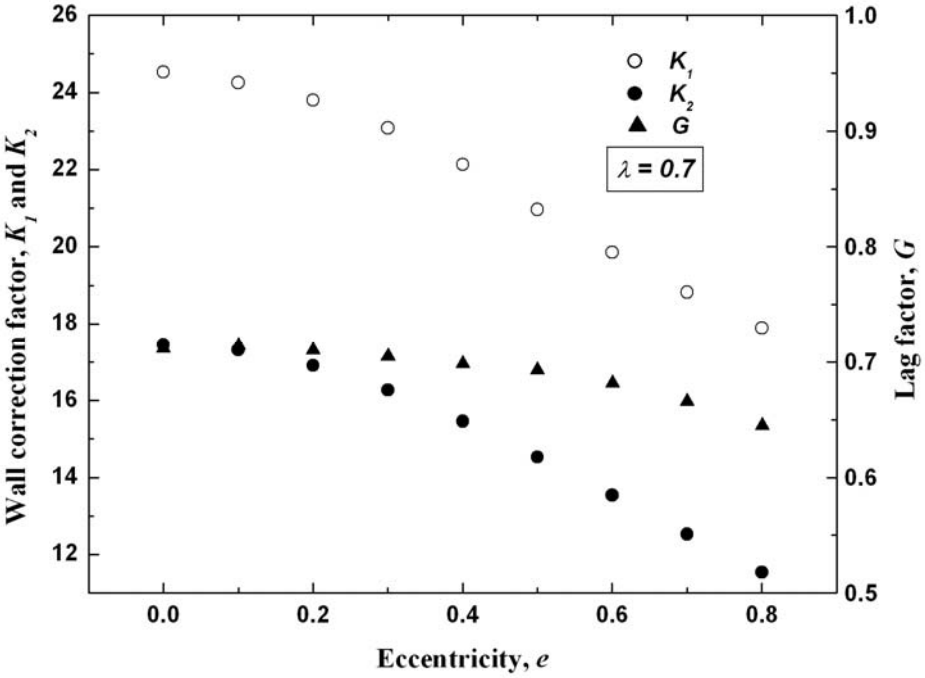

(f) Variation of wall correction factors K_1, K_2 and lag factor G for $\lambda = 0.7$

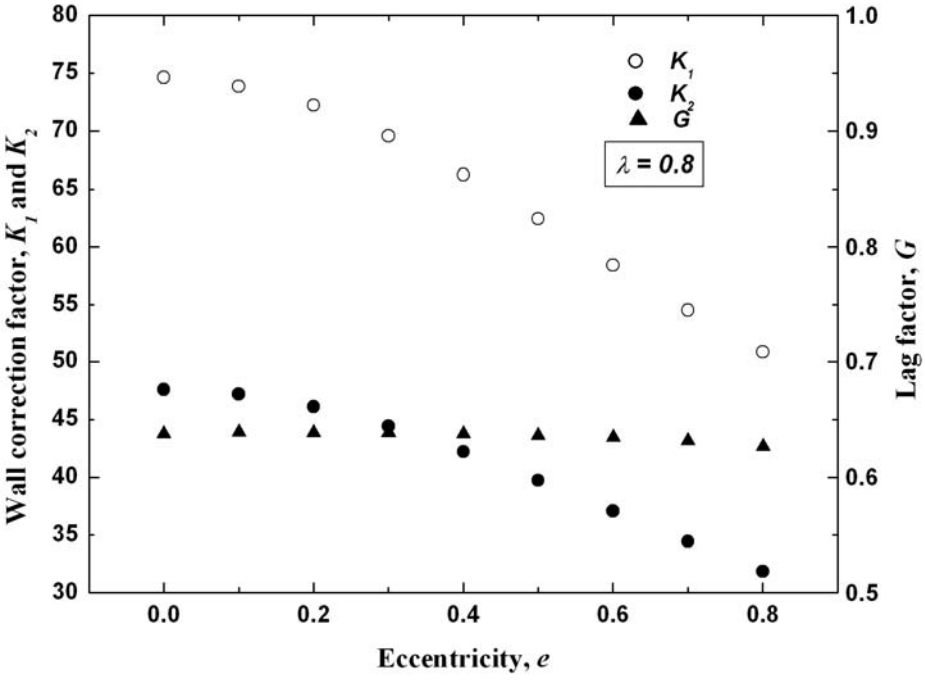

(g) Variation of wall correction factors K_1, K_2 and lag factor G for $\lambda = 0.8$

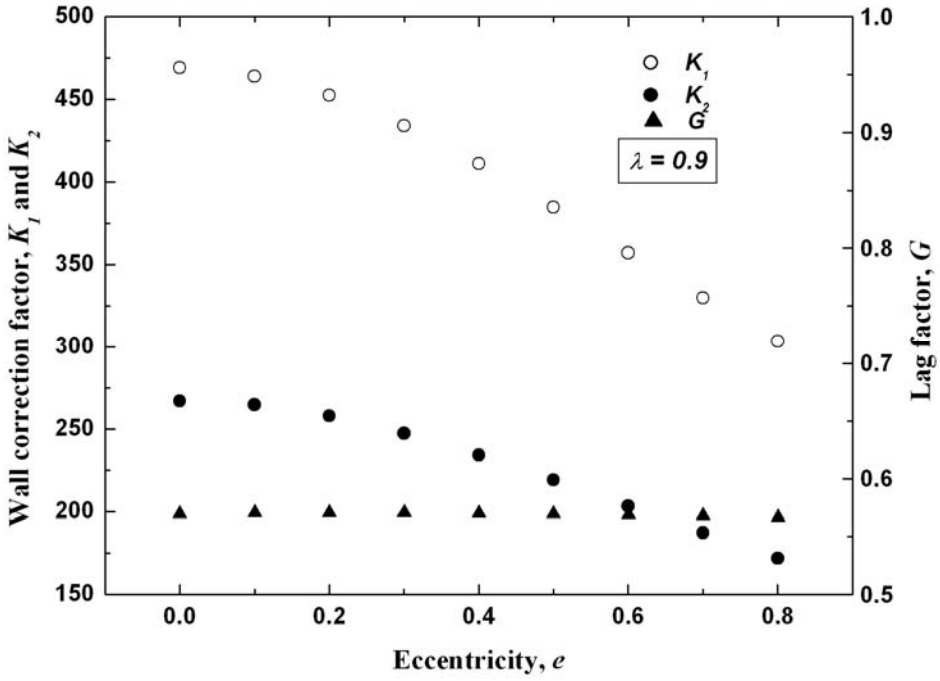

(h) Variation of wall correction factors K_1, K_2 and lag factor G for $\lambda = 0.9$

Figure 5.3: Variation of wall correction factors K_1, K_2 and lag factor G for different particle sizes with its radial position inside the channel.

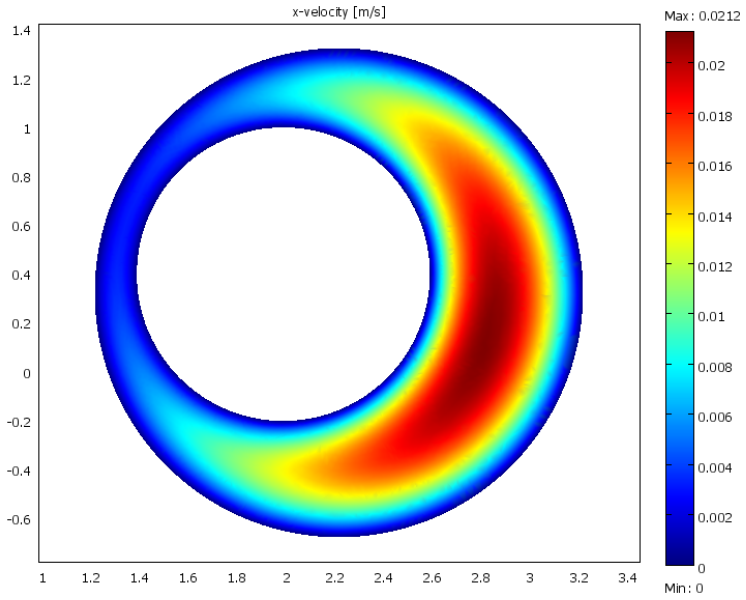

Figure 5.4: Fluid velocity at a cross section through the particle center for particle to channel radii ratio 0.6 and eccentricity 0.6.

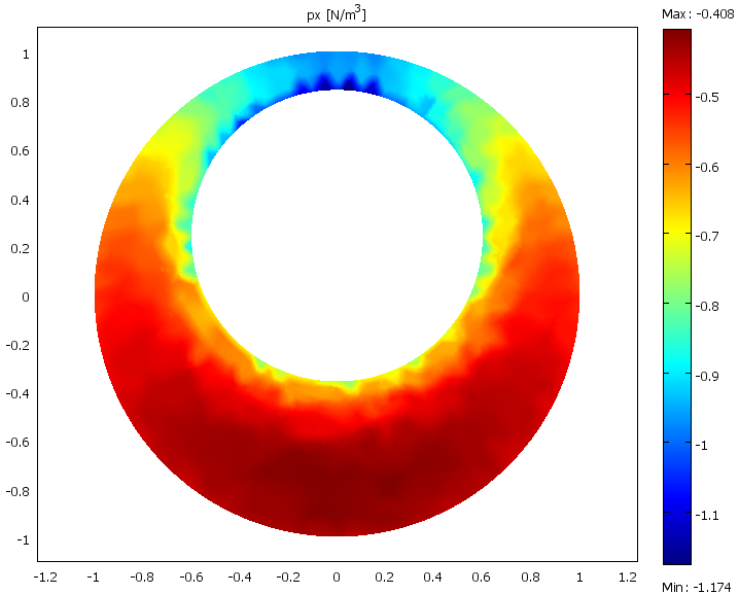

Figure 5.5: Pressure gradient at the cross section through the particle center

5.3 Effect of Size of the Particle on its Motion

Variations of K_1, K_2 and G with the radial position of the particle inside the channel for all particle to channel radii rations i.e. λ values are compared in Figure 5.6, Figure 5.7 and Figure 5.8, respectively. It is well noticeable that the variation of K_1 and K_2 follows the same trend with varying eccentricity for all particle sizes. The variation of lag factor with eccentricity for all particle sizes is compared in Fig. 5.8. It can be observed that the change in the lag factor with eccentricity is not significant for larger sized particle i.e.

particle to channel radii ratio $\lambda > 0.8$. However, for smaller sized particles change in the value of lag factor with eccentricity is significant.

The value of the lag factor decreases with the eccentricity of the particle. However, the decrease is not significant for larger particle sizes. The particle velocity remains above the mean fluid velocity at most of the eccentric positions for all particle sizes. At the highest eccentric case i.e. at $e = 1$, there is direct contact between the particle and the channel wall, which results the particle velocity to be zero. Thus the value of lag factor for a non-rotating particle should approach zero at the highest limit of the eccentricity. (However, if such contact exists, rolling of the particle on the channel surface should be investigated). This is not the same case for larger particle sizes. For the highest possible size for a spherical particle flowing axially in a cylindrical channel i.e. at $\lambda \to 1$ the particle radius is nearly equal to the channel radius and the particle would act as a piston. So, for larger sized particles the value of the lag factor remains fixed with eccentricity and does not approach to zero for higher eccentricity values.

Effect of the particle size on the variation of wall correction factor K_1 and K_2 and lag factor G for the same eccentricity value is compared in Figure 5.9, Figure 5.10 and Figure 5.11, respectively. It is observed that, K_1 and K_2 increases with particle sizes for all eccentric positions. For smaller sized particles variation in the values of K_1 and K_2 with eccentricity is lower than that occurs for larger sized particles. Change in the lag factor with eccentricity is not significant for larger sized particle, but for smaller sized particles this change is significant.

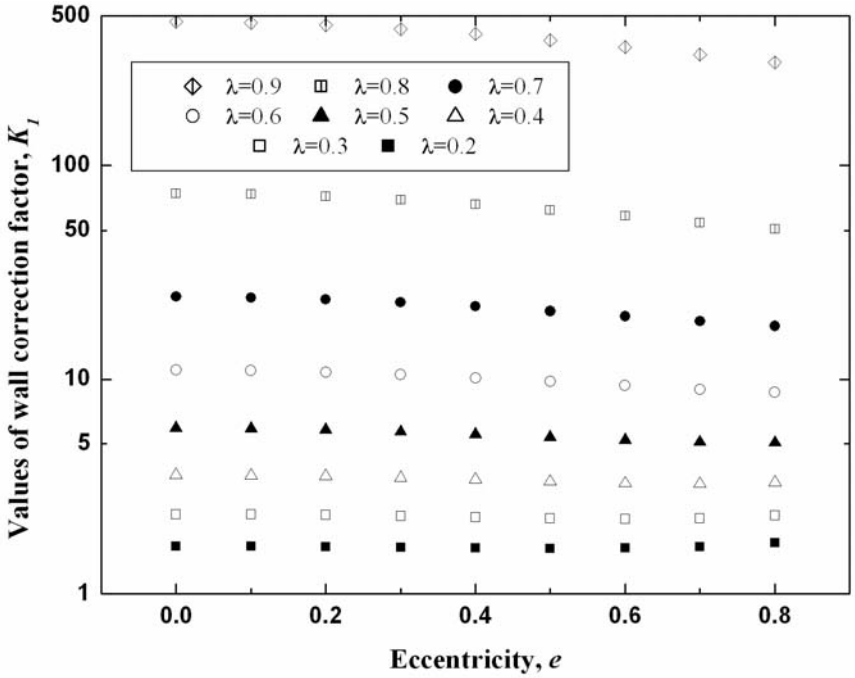

Figure 5.6: Variation of wall correction factor K_1 with radial position of the particle for different particle sizes

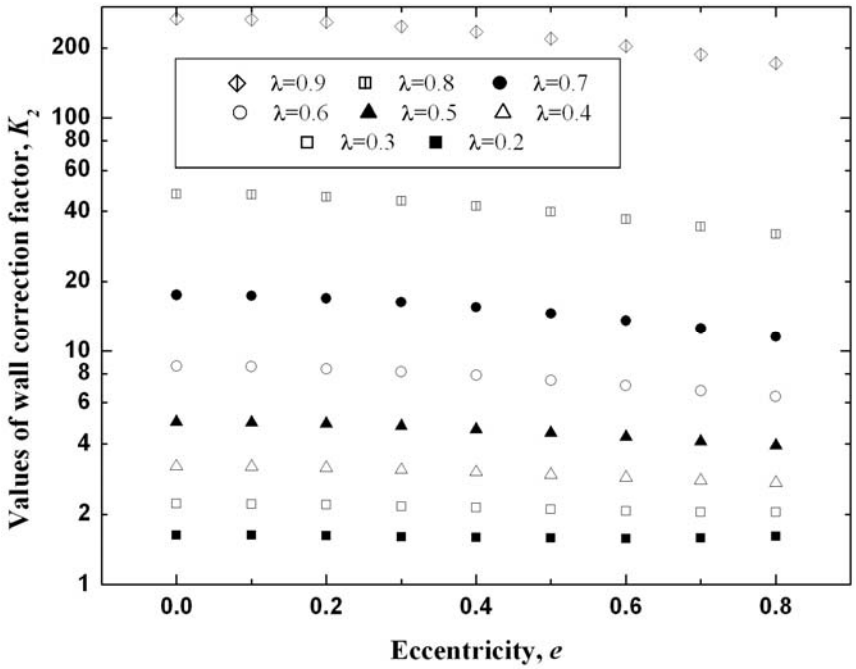

Figure 5.7: Variation of wall correction factor K_2 with radial position of the particle for different particle sizes

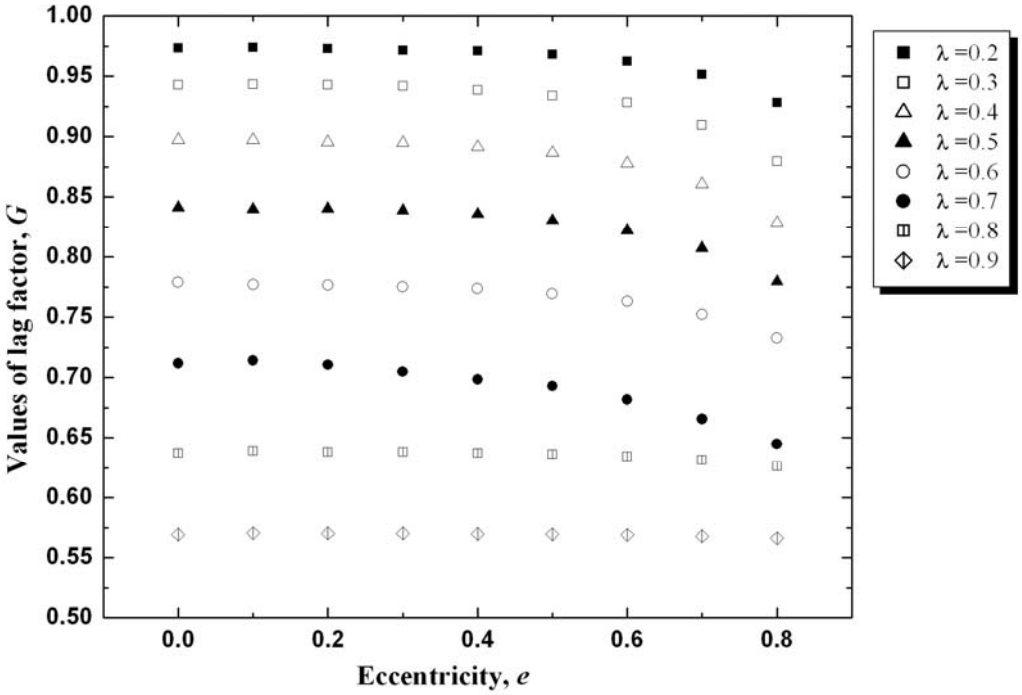

Figure 5.8: Variation of lag factor *G* with radial position of the particle for different particle sizes

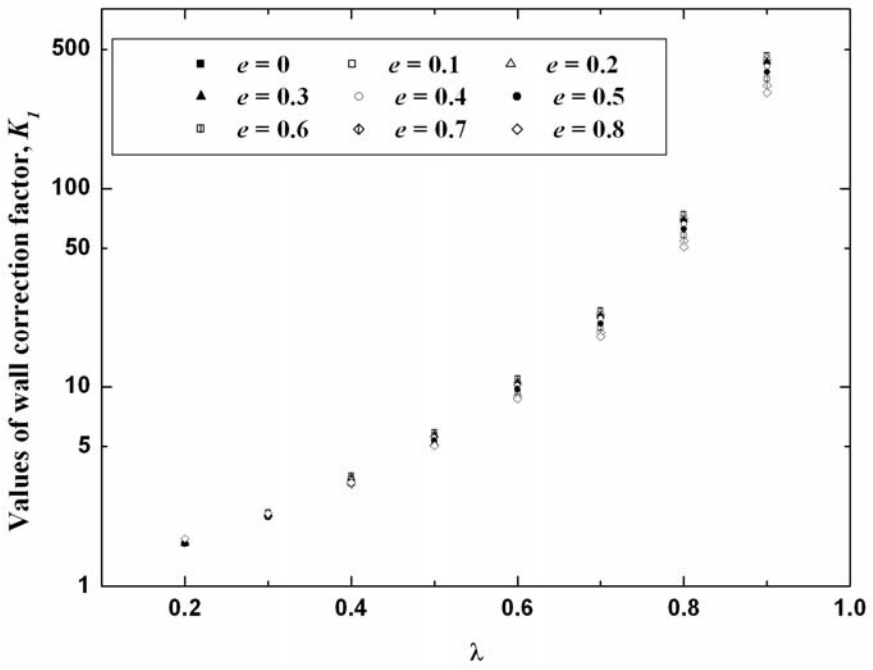

Figure 5.9: Variation of wall correction factor K_1 with particle sizes at same eccentric position.

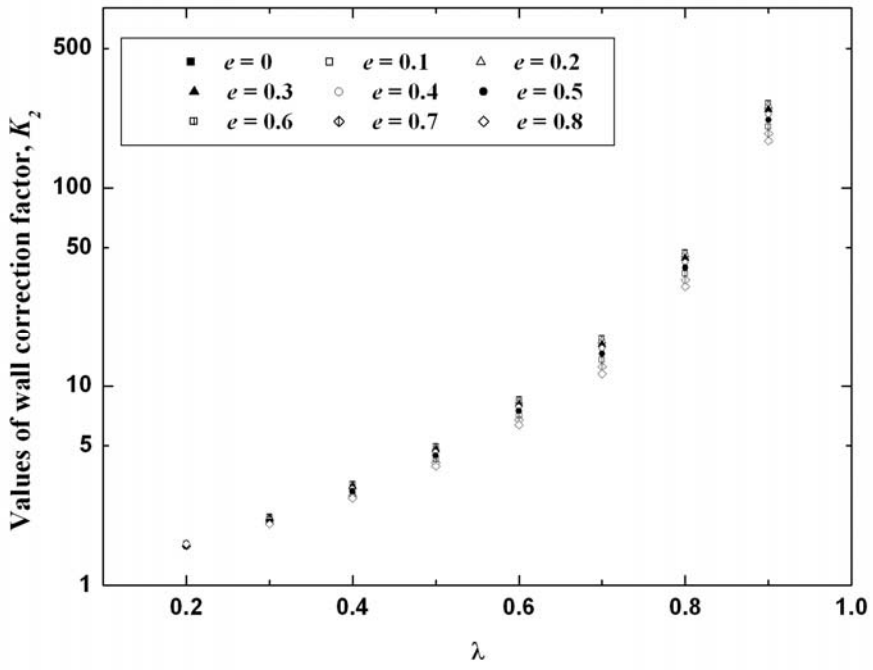

Figure 5.10: Variation of wall correction factor K_2 with particle sizes at same eccentric position.

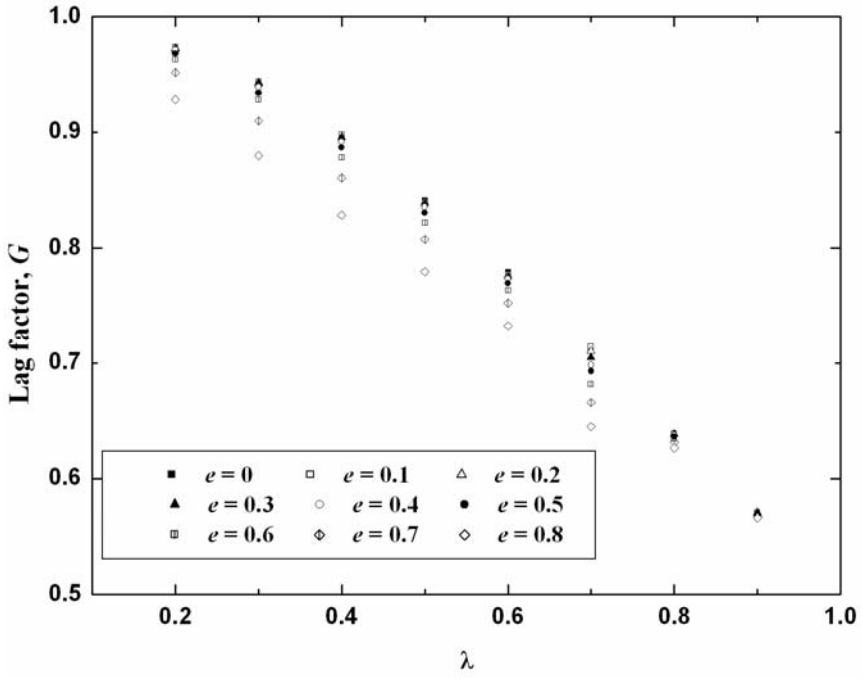

Figure 5.11: Variation of lag factor *G* with particle sizes at same eccentric position.

5.4 Comparison with Lubrication Theory Results

Calculated values of K_1, K_2 and G by NS-ALE model are compared with the values of [6] for $\lambda = 0.2$, $\lambda = 0.6$ and $\lambda = 0.9$ as are shown in Fig 5.12, Fig. 5.13 and Fig. 5.14, respectively. The solution methodology adopted in [6] is briefly described in Appendix B. Their calculated values of K_1, K_2 and G follow similar trend for all particle sizes compared to the values from NS-ALE model. Fig. 5.12 shows that, the values of K_2 calculated by [6] for $\lambda = 0.2$ decreases monotonically, while the values from NS-ALE model increase rapidly at higher eccentricity values. This is due to the fact that, in this analysis while calculating the wall correction factor K_2, local fluid velocity is used unlike in [6] where fluid velocity at the channel centerline was used.

The calculated values of wall correction factors and lag factor by the NS-ALE model are in well agreement with those calculated by the lubrication theory analysis for lower eccentricity values ($e < 0.2$) for all particle to channel radii ratios. However, with increasing eccentricity the deviation increases and values of K_1, K_2 and G from NS-ALE model are higher compared to calculated values by [6]. For smaller particle to channel radii ratios ($\lambda = 0.2$) this deviation is significant. However, for larger particle to channel radii ratios ($\lambda = 0.9$) the deviation is considerably lower at higher eccentricity values. This can be explained by the effect of separation distance of the particle from the channel wall and the curvature of the channel and particle surface. The separation distance is denoted by h and the curvature of any surface is the reciprocal of its radius.

The presumption in the lubrication theory is that, the separation distance between the particle surface and the channel wall is significantly small compared to the particle radius (i.e. $h << a$) and also to the curvature of the particle and channel surface. For larger particles, at all eccentricity values the separation of the particle surface everywhere remains small compared to the particle radius, thus the calculations of the hindrance factors by utilizing the lubrication theory are accurate. For example, for $\lambda = 0.9$, when the particle is moving along the channel centerline the normalized separation distance h/r_0 is equal to 0.1, while at eccentricity $e = 0.8$, h/r_0 is equal to 0.02. So, for larger sized particles the separation distance is considerably lower compared to the particle radius at all eccentricity values. In contrast, for smaller sized particles, for $\lambda = 0.2$, when the eccentricity value is high i.e. at $e = 0.8$, the separation distance h/r_0 is 0.16 which is of same order of the particle radius. So, for smaller sized particles the separation distance is not comparatively lower even at higher eccentricity values. This suggests the reason for deviation between the results obtained by NS-ALE model with those obtained by lubrication theory.

Moreover, the curvature of the particle and channel wall comes into play for smaller sized particles. At same eccentricity value i.e. at $e = 0.8$, the ratio of the separation distance h to the particle radius a is 0.8 and 0.025 for $\lambda = 0.2$ and $\lambda = 0.9$ respectively. As the h/a ratio is not negligible for smaller sized particles even at higher eccentricities, the effect of the curvature of the particle and channel surfaces causes the deviation of the wall correction factors using the lubrication theory.

Another factor that deserves attention to be responsible for the deviation in the calculated value of wall correction factors and the lag factors is the inertia effect on the particle motion. It was observed in [19] that the wall correction factor K_1 for the particle motion at the capped end of the channel calculated by the linear superposition of two flow regime does not conforms to the numerical calculation taking into account of the inertia effects. This suggests that the effect of inertia on the values of wall correction factors cannot be neglected fully, although the Reynolds number remains in the fully Stokes regime ($Re \leq 1 \times 10^{-3}$).

In Figure 5.15, a graphical representation of the values of lag factor G at different separation distances are given for different particle to channel radii ratios. The top and bottom boundary of the figure represents the channel wall and channel centerline, respectively. Each column stands for a specific particle size. The lag factors are written in a position equal to the separation distance of the particle from the channel wall. From this figure, a good insight of the lag factor values for each particle sizes and at different separation distance can be understood at a glance.

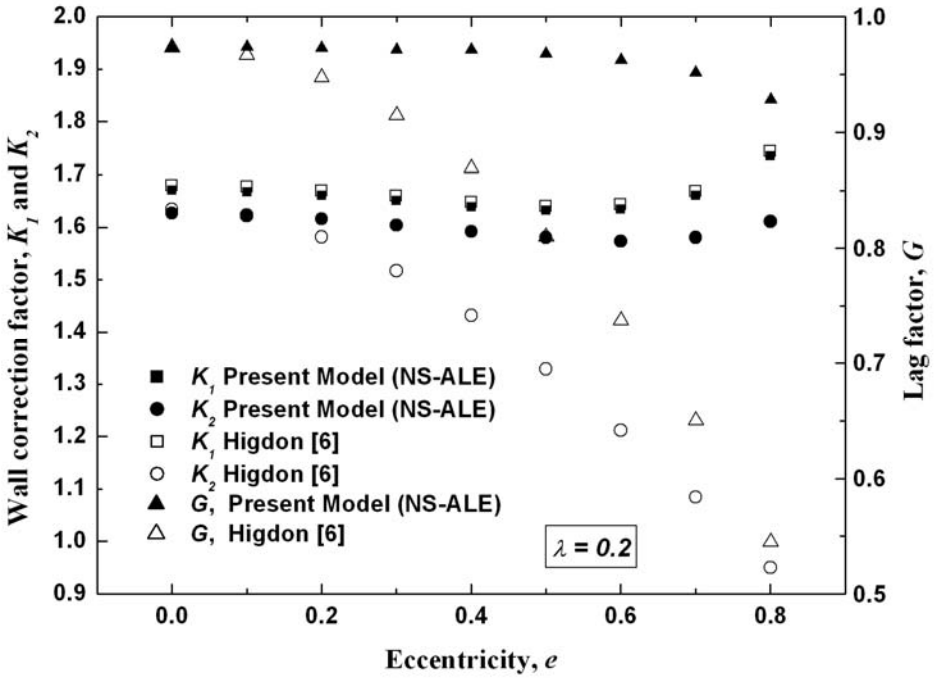

Figure 5.12: Comparison of wall correction factor K_1, K_2 and lag factor G with calculated values of Higdon and Muldowney [6] for $\lambda = 0.2$

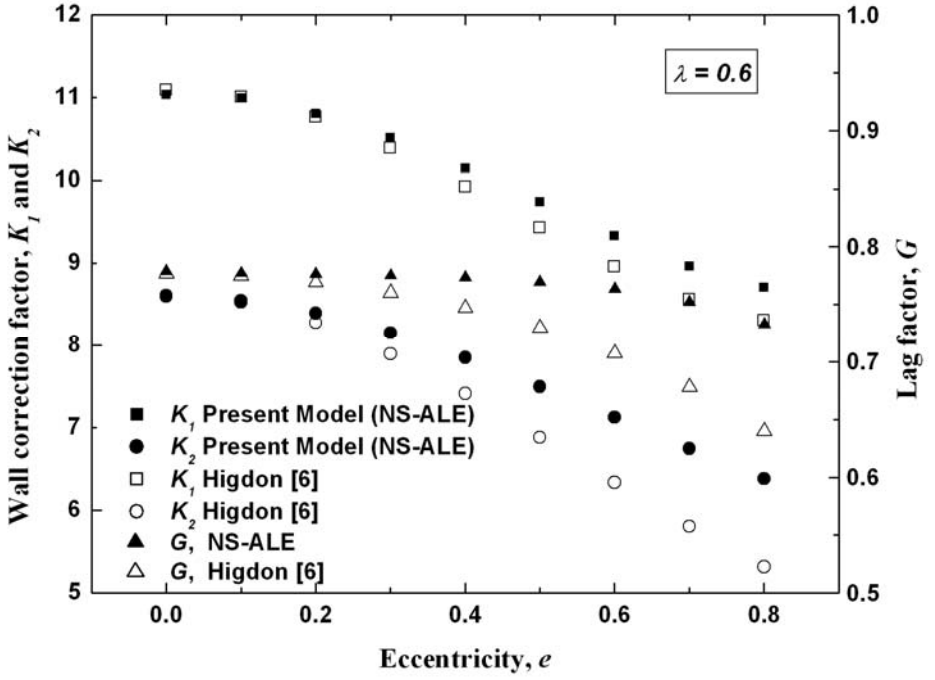

Figure 5.13: Comparison of wall correction factor K_1, K_2 and lag factor G with calculated values of Higdon and Muldowney [6] for $\lambda = 0.6$

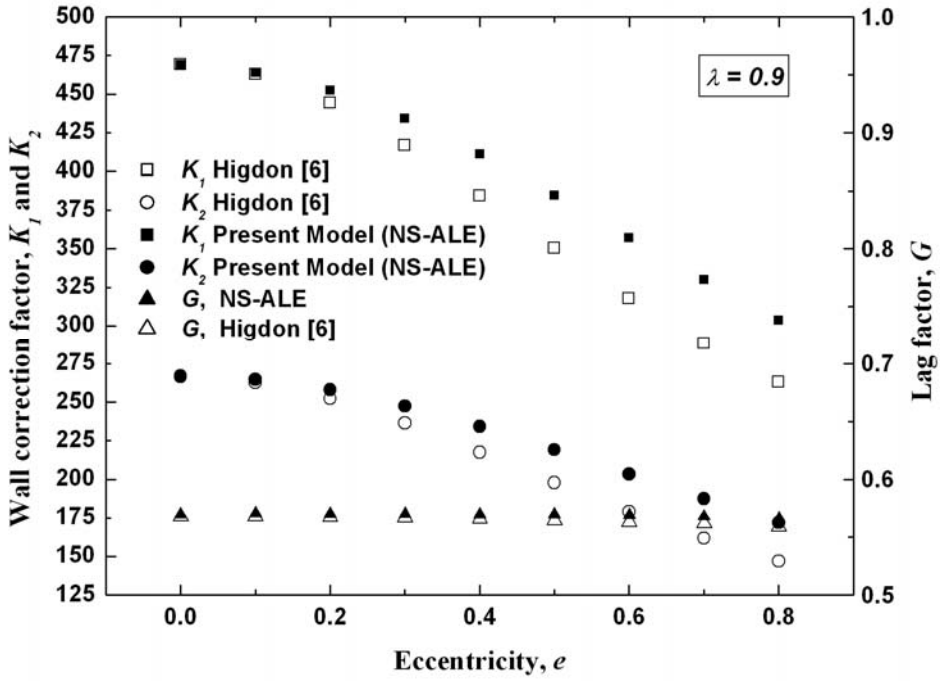

Figure 5.14: Comparison of wall correction factor K_1, K_2 and lag factor G with calculated values of Higdon and Muldowney [6] for $\lambda = 0.9$

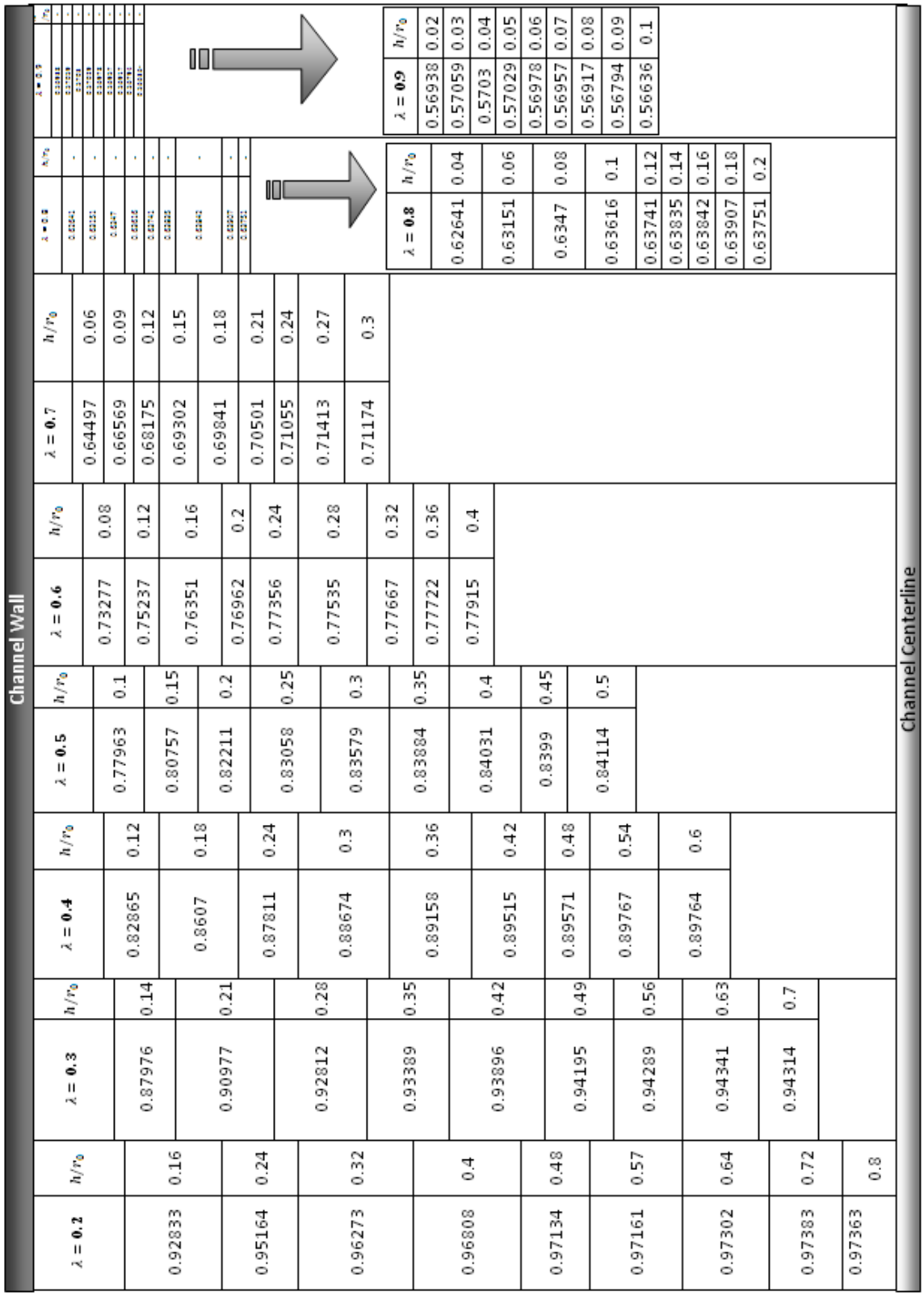

Figure 5.15: Graphical depiction of lag factor *G* at different separation distances of the particle from the channel wall

6. CONCLUSION AND RECOMMENDATIONS

6.1 Concluding Remarks

The development of the hydrodynamic theory of hindered transport for rigid uncharged spheres in pores of cylindrical cross section has reached a state of completion. Previously, centerline approximation was used to find the approximate value of overall convective flux of the particle containing fluid inside a cylindrical channel. Accurate quantitative values are now available for local enhanced drag coefficients for a sphere traveling parallel to the channel axis for all of its radial positions. Accurate value of the overall convective flux of the particle containing fluid can now be readily obtained by utilizing the radial average values of these local enhanced drag coefficients.

In this chapter, conclusions are drawn based on the analysis performed in the previous chapter. The analyses were performed first through investigating the effect of wall on the motion of a spherical particle moving along the centerline of a cylindrical channel by varying the particle to channel radii ratio λ. Later the analyses were performed for different eccentric position of the particle i.e. varying the eccentricity e of the particle.

From the results of wall correction factors and lag factors of a spherical particle of different sizes and eccentric positions, the following inferences can be drawn:

- Wall correction factors K_1 and K_2 increase with increasing particle size. The value of K_2 is always lower than the value of K_1. The physical significance of this is, drag experienced by the particle due to its motion is higher than the drag force exerted on the particle by the flowing fluid. This suggests the particle will always move slower than the flowing fluid i.e. the lag factor will always be less than unity.

- The variation of K_1 and K_2 follows the same trend with varying eccentricity. Values of wall correction factor K_1 and K_2 for larger sized particles ($\lambda > 0.3$) decreases monotonically with eccentricity. But for smaller sized particles ($\lambda < 0.3$), the values of K_1 and K_2 initially decrease and then have a tendency to increase at eccentricity value around $e = 0.6$. This increase accounts for the parabolic velocity profile of the flowing fluid.

- For all particle sizes, values of K_1, K_2 and G from NS-ALE model follow similar trend like the values of [6]. For lower eccentricity values i.e. $e < 0.2$, both results are very close. However, with increasing eccentricity the deviation increases and values of K_1, K_2 and G from NS-ALE model are higher compared to the values obtained from lubrication theory [6]. This improvement in the calculated results accounts for the consideration of the inertia effect on the particle motion in the NS-ALE model.

- Values of K_1 and K_2 increases with particle sizes for all eccentric positions. For smaller sized particles variation in the values of K_1 and K_2 with eccentricity is lower than that occurs for larger sized particles. This suggests that the centerline approximation for larger sized particles introduce more inaccuracy than that would occur for small particle sizes.

- The value of the lag factor decreases with the eccentricity of the particle. However, the decrease is not significant for larger particle sizes. The particle velocity remains above the mean fluid velocity at most of the eccentric positions for all particle sizes. The value of lag factor for small sized particles approaches zero at the highest limit of the eccentricity. However, for larger sized particles ($\lambda > 0.8$) the value of the lag factor remains fixed with eccentricity and does not approach to zero for higher eccentricity values.

6.2 Recommendations for Future Work

Some possible directions of the future works are as follows:

- Values of wall correction factors and lag factor for a spherical particle for finite Reynolds numbers are lacking in the literature. The present model can be utilized to get the accurate quantitative values of the wall correction factors and lag factor at any Reynolds number within the laminar flow region. Effect of the inertia on the particle motion can be investigated by doing the analysis at different Reynolds number.

- In this model, results were obtained for a single particle moving through the channel. A series of particle movement can be simulated for getting a true picture of particle distribution inside the channel.

- Only hydrodynamic interaction is taken into consideration here, whereas electrostatic and other physics should also be explored based on the practical interests.

- This model can be utilized to find the wall correction factors and lag factor for particles of different geometric shapes, such as, dumbbell, cylindrical, circular disk, cubes, parallelepipeds, needles and thin plates etc.

- In this research, the particles are considered to be rigid in nature. In many applications, the particles are not always rigid. Flow induced deformation should be taken into consideration for getting the results in future.

REFERENCES

[1] Ennis, J., Zhang, H., Stevens, G., Perera, J., Scales, P., Carnie, S., "Mobility of protein through a porous membrane," *Journal of Membrane Science*, vol. 119, pp. 47-58, 1996.

[2] Bear, J. and Bachmat, Y., *Introduction to modeling of transport phenomena in porous media*, Springer, 1990.

[3] Chellam, S., Wiesner, M. R., "Particle transport in clean membrane filters in laminar flow," *Environmental Science & Technology*, vol. 26, pp. 1611-1621, 1992.

[4] Cox, R. G. and Mason, S. G., "Suspended particles in fluid flow through tubes," *Annual Review of Fluid Mechanics*, vol. 3, pp. 291-316, January 1971.

[5] Bungay, P. M. and Brenner, H., "The motion of a closely fitting sphere in fluid filled tube," *Int. journal of Multiphase flow*, vol. 1, pp. 25-56, 1973.

[6] Higdon, J. J. L. and Muldowney, G. P., "Resistance functions for spherical particles, droplets and bubbles in cylindrical tubes," *Journal of Fluid Mechanics*, vol. 298, pp. 193-210, 1995.

[7] Donea, J., Huerta, A., and Ponthot, J.-P., Rodriguez-Ferran, A., "Arbitrary Lagrangian-Eulerian Methods," in Stien, E., de Borst, R., and Hughes, J. R., (Eds.), *Arbitrary Lagrangian-Eulerian methods*, Chapter 14, John Willy & Sons, 2004.

[8] Deen, W. M., "Hindered transport of large molecules in liquid-filled pores," *AIChE Journal*, vol. 33, pp. 1409-1425, 1987.

[9] Dechadilok, P. and Deen, W. M., "Hindrance factors for diffusion and convection in pores," *Ind. Eng. Chem. Res.*, vol. 45, pp. 6953-6959, 2006.

[10] Happel, J. and Brenner, H., *Low Reynolds number hydrodynamics: with special applications to particulate media*, First paperback edition, Springer, 1983.

[11] Haberman, W. L. and Sayre, R. M., "Motion of rigid and fluid spheres in stationary and moving liquids inside cylindrical tubes," U.S. Navy, David Taylor Basin, Hydromechanics Laboratory, Tech. Rep. No. 1143, 1958.

[12] Andersen, J.L., and Quinn, J.A., "Restricted transport in small pores: a model for steric exclusion and hindered particle motion," *Biophysics Journal*, vol. 14, pp. 130-150, 1974.

[13] Paine, P.L., and Scherr, P., "Drag coefficients for the movement of rigid spheres through liquid-filled cylindrical pores", *Biophysics Journal*, vol. 15, pp. 1087-1091, 1975.

[14] Bowen, W. R. and Sharif, A. O., “Transport through microfiltration membranes--particle hydrodynamics and flux reduction,” *Journal of Colloid and Interface Science*, vol. 168, pp. 4144-21, Dec. 1994.

[15] Bowen, W.R., and Sharif, A.O., “The hydrodynamic and electrostatic interactions on the approach and entry of a charged spherical particle to a charged cylindrical pore in a charged planar surface with implications for membrane separation process,” *Mathematical, Physical and Engineering Sciences*, vol. 452, pp. 2121-2140, 1996.

[16] Feng, Z. G., and Michaelides, E. E., “Hydrodynamic force on spheres in cylindrical and prismatic enclosures”, *International Journal of Multiphase Flow*, vol. 28, pp. 479-496, 2002.

[17] Ben Richou, A., Ambari, A. and Naciri, A., “Correction factor of the Stokes force undergone by a sphere in the axis of a cylinder in uniform and Poiseuille flows,” *The European Physical Journal, Applied Physics*, vol. 24, pp. 153-165, 2003.

[18] Dechadilok, P. and Deen, W. M., “Hindrance factors for diffusion and convection in pores,” *Ind. Eng. Chem. Res.*, vol. 45, pp. 6953-6959, 2006.

[19] Quddus, N. Al., Moussa, W. A. and Bhattacharjee, S., “Motion of a spherical particle in a cylindrical channel using arbitrary Lagrangian-Eulerian method,” *Journal of Colloid and Interface Science*, vol. 317, pp. 620-630, Jan. 2008.

[20] Ambari, A., Gauthier-Manuel, B. and Guyon, E., “Wall effects on a sphere translating at constant velocity”, *Journal of Fluid Mechanics*, vol. 149, pp. 235-253, 1984.

[21] Iwaoka, M., and Ishii, T., “Experimental wall correction factors of single solid spheres in triangular and square cylinders and parallel plates”, *J. Chem. Eng. Jpn*., vol. 12(3), pp. 239–242, 1979.

[22] Staben, M. E., and Davis, R. H., “Particle transport in Poiseuille flow in narrow channels,” *Int. J. Multiphase Flow*, vol. 31, pp. 529-547, 2005.

[23] Chhabra, R. P., “Wall effects on free-settling velocity of non-spherical particles in viscous media in cylindrical tubes,” *Powder Technology*, vol. 85, pp. 83-90, 1995.

[24] Shames, I. H., *Mechanics of Fluids*, fourth edition, McGraw-Hill, 2003.

[25] Duarte, F., Gormaz, R. and Natesan, S., “Arbitrary Lagrangian Eulerian method for Navier-Stokes equations with moving boundaries,” *Computer Methods in Applied Mechanics and Engineering*, vol. 193, pp. 4819-4836, 2004.

[26] Hu, H. H., Patankar, N. A. and Zhu, M. Y., “Direct numerical simulations of fluid-solid systems using the arbitrary Lagrangian-Eulerian technique,” *Journal of Computational Physics*, vol. 169, pp. 427-462, 2001.

[27] Reddy, J. N., *Finite Element Method*, third edition, Tata McGraw-Hill, 2008.

[28] Huebner, K. H., Dewhirst, D. L., Smith, D. E. and Byrom, T. G., *The finite element method for engineers*, fourth edition, John Wiley & Sons, Inc, 2004.

APPENDIX A

Navier-Stokes Equation in ALE Kinematical Description

The material domain, denoted by R_X , made up of material particles X is used as reference in Lagrangian description and the spatial domain, denoted by R_x consisting of spatial points x is used as reference in Eulerian description. The referential configuration R_χ consists of coordinate points χ is used to identify the grid points in ALE description. These three domains are related to each other by three conformal mappings φ, ϕ and ψ which is shown in the following figure

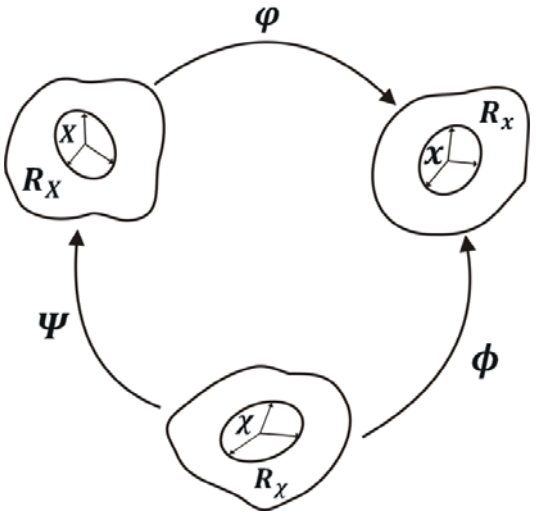

R_X : Material domain, reference for Lagrangian description

R_x : Spatial domain, reference for Eulerian description

R_χ : Referential domain, reference for ALE description

Fig. A.1: Three reference domains and the associated mappings relating those

The referential domain R_χ is mapped into the material and spatial domains by ψ and ϕ respectively and φ defines the relationship between the spatial domain and material domain. Also these three mappings are not independent. They are related to each other as:

$$\varphi = \phi * \psi^{-1} \tag{A.1}$$

The spatial coordinate x of each material point X is related by its motion and that relationship can be defined as a one to one mapping between the material domain R_X to spatial domain R_x. So φ can be described as:

$$\varphi: R_X \times [t_0, t_{final}[\longrightarrow R_x \times [t_0, t_{final}[$$

$$(X, t) \longmapsto \varphi\,(X, t) = (x, t)$$

This gives a relationship between X and x in time,

$$x = x(X, t), \qquad t = t$$

The gradient of the mapping φ can be expressed in matrix form as:

$$\frac{\delta\varphi}{\delta(X,t)} = \begin{pmatrix} \frac{\delta x}{\delta X} & v \\ 0^T & 1 \end{pmatrix} \tag{A.2}$$

Here v is the material velocity and can be given by:

$$v(X,t) = \left.\frac{\delta x}{\delta t}\right|_{\boldsymbol{X}} \tag{A.3}$$

Here $|_{\boldsymbol{X}}$ means holding the material coordinate fixed. So, it defines the velocity of a specific material particle.

Similarly the mapping ϕ from the referential domain to the spatial domain can be understood as the motion of the grid points in the spatial domain and is represented by:

$$\phi: R_{\boldsymbol{\chi}} \times [t_0, t_{final}[\;\longrightarrow R_x \times [t_0, t_{final}[$$

$$(\boldsymbol{\chi}, t) \longmapsto \phi\,(\boldsymbol{\chi}, t) = (x, t)$$

The gradient of this mapping can be represented in matrix form as:

$$\frac{\delta\phi}{\delta(\boldsymbol{\chi},t)} = \begin{pmatrix} \frac{\delta x}{\delta \boldsymbol{\chi}} & \hat{v} \\ 0^T & 1 \end{pmatrix} \tag{A.4}$$

here, $\hat{v}$ is the mesh velocity and can be expressed as:

$$\hat{v}(\boldsymbol{\chi}, t) = \left.\frac{\delta x}{\delta t}\right|_{\boldsymbol{\chi}} \tag{A.5}$$

One important point to note here, in Lagrangian viewpoint, since the material points coincide with the same grid points during the whole motion, there are no convective effects. In Eulerian viewpoint, the mesh nodes are not attached with the material particles, so convective effects arise and the convective velocity i.e. the relative velocity between mesh nodes and material points is simply the velocity of the material points. However, in arbitrary Lagrangian Eulerian viewpoint both the reference domain and material domain are moving with respect to spatial domain. So, in this description the convective velocity need to be determined.

The mapping ψ defines the relationship between the referential domain and the material domain. This is of particular interest because by varying the definition of this mapping both the Eulerian and Lagrangian description can be achieved. It is convenient here to write its direct inverse ψ^{-1} as:

$$\psi^{-1}: R_X \times [t_0, t_{final}[\longrightarrow R_\chi \times [t_0, t_{final}[$$

$$(X, t) \longmapsto \psi^{-1}(X, t) = (\boldsymbol{\chi}, t)$$

The gradient of mapping ψ^{-1} can be expressed as:

$$\frac{\delta \psi^{-1}}{\delta (X, t)} = \begin{pmatrix} \frac{\delta \boldsymbol{\chi}}{\delta X} & w \\ 0^T & 1 \end{pmatrix} \tag{A.6}$$

here, the velocity w is:

$$w = \left. \frac{\delta \boldsymbol{\chi}}{\delta t} \right|_X \tag{A.7}$$

This w can be interpreted as the particle velocity in the referential domain.

The relation between v, $\hat{v}$ and w is found by differentiating equation $\varphi = \phi * \psi^{-1}$.

$$\frac{\delta \varphi}{\delta (X, t)}(X, t) = \frac{\delta \phi}{\delta (\boldsymbol{\chi}, t)} \left(\psi^{-1}(X, t) \right) * \frac{\delta \psi^{-1}}{\delta (X, t)}(X, t)$$

$$= \frac{\delta \phi}{\delta (\boldsymbol{\chi}, t)} (\boldsymbol{\chi}, t) * \frac{\delta \psi^{-1}}{\delta (X, t)}(X, t)$$

This can be represented in matrix form as:

$$\begin{pmatrix} \frac{\delta x}{\delta X} & v \\ 0^T & 1 \end{pmatrix} = \begin{pmatrix} \frac{\delta x}{\delta \boldsymbol{\chi}} & \hat{v} \\ 0^T & 1 \end{pmatrix} * \begin{pmatrix} \frac{\delta \boldsymbol{\chi}}{\delta X} & w \\ 0^T & 1 \end{pmatrix},$$

which yields after multiplication:

$$v = \hat{v} + \frac{\delta x}{\delta \boldsymbol{\chi}} \cdot w \tag{A.8}$$

The above equation can be rewritten as:

$$v - \hat{v} = \frac{\delta x}{\delta \boldsymbol{\chi}} \cdot w \tag{A.9}$$

This is the convective velocity i.e. the difference between the mesh velocity and material velocity.

Now, the time derivative of any physical quantity in the referential domain needs to be discussed, because in the Navier-Stokes equation there is a term representing time derivative of velocity. The time derivative of any physical quantity $\boldsymbol{u}$ for a given

particle X i.e. its material derivative can be expressed as the summation of its local derivative (with the reference coordinate held fixed) and the convective term taking into account the relative velocity between the material and the reference system. This is similar to the typical Eulerian framework and can be written as:

$$\left.\frac{\delta \boldsymbol{u}}{\delta t}\right|_{X} = \left.\frac{\delta \boldsymbol{u}}{\delta t}\right|_{\chi} + (v - \hat{v}) \cdot \nabla \boldsymbol{u} \tag{A.10}$$

So, the only change that will occur in the Navier-Stokes equation with respect to the referential domain, is in the convective term with the convective velocity being equal to $v - \hat{v}$. However, the continuity equation will remain the same. The resulting equations are shown below:

$$\rho\left(\left.\frac{\delta \boldsymbol{u}}{\delta t}\right|_{\chi} + (\boldsymbol{v} - \hat{\boldsymbol{v}}) \cdot \nabla \boldsymbol{u}\right) = -\nabla p + \mu \nabla \cdot (\nabla \boldsymbol{u} + \nabla \boldsymbol{u}^{T}) + \boldsymbol{F}_{b}, \tag{A.11}$$

$$\nabla \cdot \boldsymbol{u} = 0 \tag{A.12}$$

It should be noted that the equation is similar to the Eulerian equations and can be solved in a similar way in the referential domain. Here $\hat{\boldsymbol{v}}$ is the mesh velocity and from now on it is denoted by $\boldsymbol{\psi_m}$ for convenience. So the Navier Stokes equation in arbitrary Lagrangian Eulerian framework can be finally written as:

$$\rho\left(\left.\frac{\delta \boldsymbol{u}}{\delta t}\right|_{\chi} + (\boldsymbol{v} - \boldsymbol{\psi_m}) \cdot \nabla \boldsymbol{u}\right) = -\nabla p + \mu \nabla \cdot (\nabla \boldsymbol{u} + \nabla \boldsymbol{u}^{T}) + \boldsymbol{F}_{b}, \tag{A.13}$$

APPENDIX B

B.1 Solution Methodology Utilized in [6]

Stokes equation was solved using the boundary integral method. The calculated results are represented using algebraic equations for the entire position of the particle within the channel. In selecting the algebraic form used to represent the resistance functions, analytical results for three distinct regimes were utilized: (i) particles near the centre, $d/r_0 \ll 1$, (ii) small particles in the vicinity of the wall $d/r_0 \sim 1$, $a/(r_0 - d) \ll 1$, and (iii) particles in the lubrication regime where the ratio of gap size to particle radius is small, $(r_0 - d - a)/a \ll 1$**.** In region (i), the method of reflections and asymptotic analysis show that the resistance functions are even functions of d/r_0 . In region (ii), method of reflections calculations give resistance functions as power series in $a/(r_0 - d)$. In region (iii), lubrication theory yields the functional form and limiting behavior of the resistance functions.

A dimensionless position variable or eccentricity is defined as expressed by, $e = d/(r_o - a)$. Motivated by the behavior in region (ii), a dimensionless variable ρ is defined to characterize the distance of a small particle from the cylinder wall. Here, $1/\rho$ is defined as a even function of e.

$$\frac{1}{\rho} = \frac{a}{r_0}\left[1 - e^2\,(1 - \frac{a}{r_0})^2\right]^{-1}$$

A dimensionless variable δ is defined to characterize the gap size in the lubrication limit. Again it is defined as the even function of e:

$$\delta = \frac{1}{2}\,\frac{r_0}{a}\left(1 - \frac{a}{r_0}\right)\,(1 - e^2)$$

Note that δ scales as the ratio of gap/particle radius in the limit as $e \to 1$, i.e. as the gap approaches zero. For convenience, δ_0 is defined to be the value of δ evaluated at $e = 0$ which yields $\delta_0 = (r_0 - a)/2a$. With these specifications, the following approximating functions are defined:

$$\psi_0 = 1; \quad \psi_1 = \frac{a}{r_0}\,e^2\,; \quad \psi_2 = \frac{a}{r_0}\,e^4\,;$$

$$\psi_3 = e^{2m}\frac{e^2}{\rho}\;\;;$$

$$\psi_4 = e^{2m}\left(\frac{e^2}{\rho}\right)^2\;;$$

$$\psi_5 = \delta \left[\ln\left(\frac{\delta+1}{\delta}\right) - \ln\left(\frac{\delta_0+1}{\delta_0}\right)\right] - e^2 \left(\frac{\delta_0}{\delta_0+1}\right);$$

$$\psi_6 = \left[\ln\left(\frac{\delta+1}{\delta}\right) - \ln\left(\frac{\delta_0+1}{\delta_0}\right)\right] - e^2 \left(\frac{1}{\delta_0+1}\right);$$

$$\psi_7 = \frac{1}{\delta} - \frac{1+e^2}{\delta_0};$$

The resistance functions are represented as a single continuous function over the entire range $0 < e < 1$. This decision dictates the form of the approximating functions ψ_i. The first three terms ψ_0, ψ_1, ψ_2 are determined by the asymptotic behaviour at small e. The next two terms ψ_3, ψ_4 take the form of the method of reflections contributions in region (ii) with the additional factors of e^2 to preserve the approximation in the small e limit. The last three terms ψ_5, ψ_6, ψ_7 are determined by lubrication theory. As $\delta \to 0$, these terms scale as $\delta \ln \delta$, $\ln \delta$ and $1/\delta$ respectively. In these three cases, the function ψ is defined by taking the appropriate lubrication result and subtracting the limiting behaviour for small e. As before, this serves to preserve the character of the approximation at small e.

The value of K_1 is presented in the following form:

$$K_1 = \sum_{i=0}^{7} c_i \left(\frac{a}{r_0}\right) \psi_i \left(e, \frac{a}{r_0}\right)$$

And the value of K_2 is presented in the form:

$$K_2 = \sum_{i=0}^{4} c_i \left(\frac{a}{r_0}\right) \psi_i \left(e, \frac{a}{r_0}\right) - e^2 \left(1 - \frac{a}{r_0}\right)^2$$

Values of c_i and exponent m are given in a tabulated form. The value of the exponent m is taken to be 2. Here, the values of the coefficients are shown partially for particle to channel radii ratios, $\lambda = 0.2,\ 0.6$ and $\lambda = 0.9$ only in Table B.1 and Table B.2.

Table B.1: Values of the coefficients for calculating K_1

a/r_0	c_0	c_1	c_2	c_3	c_4	c_5	c_6
0.2	1.679480	-1.30422	1.03602	-0.06911	-0.10952	-0.06961	0.58844
0.6	11.091896	-14.32557	13.86957	-8.22332	4.11603	-1.73070	0.93008
0.9	469.222507	-732.58970	1252.70861	-979.70668	645.77045	7400.80980	2.04018

Table B.2: Values of the coefficients for calculating K_2

a/r_0	c_0	c_1	c_2	c_3	c_4
0.2	1.634787	-3.55069	2.67484	-0.58220	0.63431
0.6	8.613008	-14.19404	13.70181	-8.49174	5.01887
0.9	266.432020	-417.14394	557.34338	-477.12013	208.22109

B.2 Lubrication Theory:

Here expressions for the asymptotic form of the resistance functions based on lubrication theory for two surfaces in near contact are presented.

Consider two surfaces in near contact such that the minimum distance between the surfaces is h. One surface, designated the wall, is assumed to be rigid and motionless, while the other surface designated the particle may be either fluid or solid. Assume that each surface has finite curvature at the point of minimum separation and that the curvature is much less than $1/h$, . Define a local Cartesian coordinate system with the origin on the wall at the point of nearest approach and the x-axis normal to the surfaces pointing toward the particle.

Let the rigid boundary wall be represented locally by

$$x = \eta_w = A_w\, y^2 + B_w\, z^2$$

and, the particle surface is represented by

$$x = \eta_p = h_0 + A_p\, y^2 + B_p\, z^2$$

Define, $h(y,z)$ as the gap between the walls

$$h(y,z) = \eta_p - \eta_w = h_0 + A\, y^2 + B\, z^2$$

and, define a variable $\xi = x - \eta_w$ such that the surface between the surfaces occupies the region $0 < \xi < h$.

Assume that $h_0 A,\ h_0 B \ll 1$ and note that changes in y and z scales with $1/A$ and $1/B$ while changes in x scale with h_0 . Under these circumstances, the lubrication approximation for the Stokes equations leads to the simplified form,

$$\frac{\delta p}{\delta x} = 0,\quad \frac{\delta p}{\delta y} = \mu\,\frac{\delta^2 v}{\delta x^2},\quad \frac{\delta p}{\delta z} = \mu\,\frac{\delta^2 w}{\delta x^2}$$

Now consider the shearing flow of a rigid particle. Assume that the particle velocity at the centre of the sphere is $u = (0, V, W)$ and the angular velocity is $\Omega = (0,\ \Omega_2,\ \Omega_3)$. The particle velocity at the contact point $(h_0, 0, 0)$ is then $\left(0, \breve{V}, \breve{W}\right) = (0,\ V -$

$\Omega_3 a,\ W + \Omega_2\, a\,)$. The no slip at the stationary wall is $u = (0,0,0)$ at $\xi = 0$. The no slip condition on the particle can be expressed as $u = (\Omega_2\, z - \Omega_3\, y, \breve{\mathrm{V}}, \breve{\mathrm{W}})$ at $\xi = h$.

Now, integrating the Stokes equation twice, employing the boundary conditions and substituting the velocity components a lubrication equation for p is found, which yields,

$$p = (k_2 y + k_3\, z)/\, h^2$$

The no-slip boundary condition yield values for the coefficients k_2 and k_3 in terms of V, W, Ω_2 and Ω_3. Evaluating the force and torque on the particle, a zero torque condition is employed to solve for Ω_2 and Ω_3. The final results for the force on a torque-free rigid particle are,

$$K_1 = \frac{F_z}{6\pi\mu a W} = 2\left(\frac{r_0}{4r_0 - a}\right)\left(\frac{r_0}{r_0 - a}\right)^{1/2} \ln\left(\frac{a}{h_0}\right)$$

This equation provides the values for the coefficients c_6 in the table B.1 shown above.